Scientific Research from the Ministry of Health, Labour and Welfare of Japan and the Ministry of Education, Culture, Sports, Science and Technology of Japan (#19591075, 21591176, 21119013, and 21390533). The authors declare no potential conflicts of interest with respect to the authorship and/or publication of this article.

REFERENCES

Arron JR, Winslow MM, Polleri A, Chang CP, Wu H, Gao X, *et al.* (2006). NFAT dysregulation by increased dosage of DSCR1 and DYRK1A on chromosome 21. *Nature* 441:595-600.

Chusho H, Tamura N, Ogawa Y, Yasoda A, Suda M, Miyazawa T, *et al.* (2001). Dwarfism and early death in mice lacking C-type natriuretic peptide. *Proc Natl Acad Sci USA* 98:4016-4021.

Kake T, Kitamura H, Adachi Y, Yoshioka T, Watanabe T, Matsushita H, *et al.* (2009). Chronically elevated plasma C-type natriuretic peptide level stimulates skeletal growth in transgenic mice. *Am J Physiol Endocrinol Metab* 297:E1339-E1348.

Lei WY, Wong RW, Rabie AB (2008). Factors regulating endochondral ossification in the spheno-occipital synchondrosis. *Angle Orthod* 78:215-220.

Lenton K, James AW, Manu A, Brugmann SA, Birker D, Nelson ER, *et al.* (2011). Indian hedgehog positively regulates calvarial ossification and modulates bone morphogenetic protein signaling. *Genesis* 49:784-796.

Nakao K, Ogawa Y, Suga S, Imura H (1992). Molecular biology and biochemistry of the natriuretic peptide system. I: Natriuretic peptides. *J Hypertens* 10:907-912.

Nie X, Luukko K, Kettunen P (2006). BMP signalling in craniofacial development. *Int J Dev Biol* 50:511-521.

Oka K, Oka S, Sasaki T, Ito Y, Bringas P Jr, Nonaka K, *et al.* (2007). The role of TGF-beta signaling in regulating chondrogenesis and osteogenesis during mandibular development. *Dev Biol* 303:391-404.

Richtsmeier JT, Baxter LL, Reeves RH (2000). Parallels of craniofacial maldevelopment in Down syndrome and Ts65Dn mice. *Dev Dyn* 217:137-145.

Singh GD (1999). Morphologic determinants in the etiology of class III malocclusions: a review. *Clin Anat* 12:382-405.

Suga S, Nakao K, Hosoda K, Mukoyama M, Ogawa Y, Shirakami G, *et al.* (1992). Receptor selectivity of natriuretic peptide family, atrial natriuretic peptide, brain natriuretic peptide, and C-type natriuretic peptide. *Endocrinology* 130:229-239.

Takano T, Takigawa M, Shirai E, Nakagawa K, Sakuda M, Suzuki F (1987). The effect of parathyroid hormone (1-34) on cyclic AMP level, ornithine decarboxylase activity, and glycosaminoglycan synthesis of chondrocytes from mandibular condylar cartilage, nasal septal cartilage, and spheno-occipital synchondrosis in culture. *J Dent Res* 66:84-87.

Takigawa M, Okada M, Takano T, Ohmae H, Sakuda M, Suzuki F (1984). Studies on chondrocytes from mandibular condylar cartilage, nasal septal cartilage, and spheno-occipital synchondrosis in culture. I. Morphology, growth, glycosaminoglycan synthesis, and responsiveness to bovine parathyroid hormone (1-34). *J Dent Res* 63:19-22.

Tamura N, Doolittle LK, Hammer RE, Shelton JM, Richardson JA, Garbers DL (2004). Critical roles of the guanylyl cyclase B receptor in endochondral ossification and development of female reproductive organs. *Proc Natl Acad Sci USA* 101:17300-17305.

Wealthall RJ, Herring SW (2006). Endochondral ossification of the mouse nasal septum. *Anat Rec A Discov Mol Cell Evol Biol* 288:1163-1172.

Yasoda A, Komatsu Y, Chusho H, Miyazawa T, Ozasa A, Miura M, *et al.* (2004). Overexpression of CNP in chondrocytes rescues achondroplasia through a MAPK-dependent pathway. *Nat Med* 10:80-86.

Bone 50 (2012) 69–78

Contents lists available at SciVerse ScienceDirect

Bone

journal homepage: www.elsevier.com/locate/bone

Original Full Length Article

Id2 controls chondrogenesis acting downstream of BMP signaling during maxillary morphogenesis

Tomoko Sakata-Goto [a], Katsu Takahashi [a,*], Honoka Kiso [a], Boyen Huang [a], Hiroko Tsukamoto [a], Mitsuru Takemoto [b], Tatsunari Hayashi [c], Manabu Sugai [c], Takashi Nakamura [b], Yoshifumi Yokota [d], Akira Shimizu [c], Harold Slavkin [e], Kazuhisa Bessho [a]

[a] Department of Oral and Maxillofacial Surgery, Graduate School of Medicine, Kyoto University, Japan
[b] Department of Orthopedic Surgery, Kyoto University Hospital, Japan
[c] Translation Research Center, Kyoto University Hospital, Japan
[d] Division of Molecular Genetics, Department of Biochemistry and Bioinformative Sciences, Faculty of medical Sciences, University of Fukui, Japan
[e] Center for Craniofacial Molecular Biology, School of Dentistry, University of Southern California, USA

ARTICLE INFO

Article history:
Received 3 June 2011
Revised 3 September 2011
Accepted 16 September 2011
Available online 1 October 2011

Edited by: R. Baron

Keywords:
Id2
Synchondrosis
BMP
Smad7
Jaw deformity

ABSTRACT

Maxillofacial dysmorphogenesis is found in 5% of the population. To begin to understand the mechanisms required for maxillofacial morphogenesis, we employed the inhibitors of the differentiation 2 (Id2) knock-out mouse model, in which Id proteins, members of the regulator of basic helix–loop–helix (bHLH) transcription factors, modulate cell proliferation, apoptosis, and differentiation.

We now report that spatially-restricted growth defects are localized at the skull base of Id2 KO mice. Curiously, at birth, neither the mutant Id2 KO nor wild-type (WT) mice differed, based upon cephalometric and histological analyses of cranial base synchondroses. In postnatal week 2, a narrower hypertrophic zone and an inhibited proliferative zone in presphenoid synchondrosis (PSS) and spheno-occipital synchondrosis (SOS) with maxillary hypoplasia were identified in the Id2 mutant mice. Complementary studies revealed that exogenous bone morphogenetic proteins (BMPs) enhanced cartilage growth, matrix deposition, and chondrocyte proliferation in the WT but not in the mutant model. Id2-deficient chondrocytes expressed more Smad7 transcripts.

Based on our results, we assert that Id2 plays an essential role, acting downstream of BMP signaling, to regulate cartilage formation at the postnatal stage by enhancing BMP signals through inhibiting Smad7 expression. As a consequence, abnormal endochondral ossification was observed in cranial base synchondroses during the postnatal growth period, resulting in the clinical phenotype of maxillofacial dysmorphogenesis.

Introduction

Temporal and spatial information is critical for craniofacial morphogenesis, especially between forming the mandible and complementary maxilla. In human craniofacial development, morphospatial disharmony between the maxillocranial and mandibular complex results in well-recognized jaw deformities, including maxillary hypoplasia, mandibular prognathism, mandibular micrognathism, and facial asymmetry [1]. Patients with severe jaw deformities present significant masticatory dysfunctions and severe psychosocial issues. Such patients require surgical correction and postsurgical rehabilitation. The prevalence of such jaw deformities ranges from 1 to 23% according to the ethnic background of study populations [2–5]. Jaw deformities become apparent after birth, as well as being associated with first and second branchial arch syndromes, including Treacher Collins syndrome, Pierre Robin syndrome, Crouzon syndrome, cleidocranial dysplasia (CCD), achondroplasia, and Pfeiffer syndrome. These relatively rare branchial arch syndromes are readily identified at birth, and these represent less than 5% of jaw deformity cases [1]. The vast majority of such cases become clinically evident during early postnatal growth and development. Overt manifestation of the postnatal jaw deformities may not appear until after adolescence, being generally associated with increased craniofacial growth. Both environmental and genetic factors have been identified as causes of postnatal jaw deformities [6,7], and available evidence suggests that genetic factors are the major determinants to the clinical phenotype [8–10]. However, the primary cause for maxillofacial dysmorphogenesis is not known.

In order to investigate growth impairment in postnatal jaw deformities, we identified the role of cartilages in the growth and development of the craniofacial complex. Available evidence suggests that SOS and nasal septal cartilage (NSC) are derived from the chondrocranium

* Corresponding author at: Katsu Takahashi: Shogoin-Kawahara-cho 54, Sakyo-ku, Kyoto, 606-8507, Japan. Fax: +81 75 761 9732.
E-mail address: takahask@kuhp.kyoto-u.ac.jp (K. Takahashi).

8756-3282/$ – see front matter © 2011 Elsevier Inc. All rights reserved.
doi:10.1016/j.bone.2011.09.049

[11]. Multiple synchondroses separating bones of the skull base are assumed to function as growth sites during skull base expansion. Morphologically, a synchondrosis appears at two opposing cartilage growth plates. Therefore, analogous to endochondral growth plates in long bones, synchondroses of the skull base develop through aberrations of the temporal and spatial combination of chondrocyte proliferation and hypertrophy [7]. In a mouse model, both the PSS and SOS remain patent through adulthood. Similar to the epiphyseal growth plate in long bones, the cell proliferation, differentiation, and maturation rates of chondrocytes within synchondroses are critical for the longitudinal growth of the cranial base [12].

Id proteins are members of the regulator of helix–loop–helix (HLH) transcription factors [13–15]. Transcriptional regulators with a bHLH domain regulate a broad range of cellular differentiation processes including myogenesis, neurogenesis, and hematopoiesis [16]. In embryonic and adult tissues, Id proteins act as regulators of cell proliferation, differentiation, tumorigenesis, and neoplastic transformation [17–19]. Id expression is partially regulated by BMP-Smad signaling [20,21]. BMP regulates cell fate determination, differentiation, proliferation, maturation, hypertrophy, and apoptosis of chondrocyte cells [22]. The mechanisms by which BMPs control specific cell lineages and patterns have been found to be critical for subsequent stages of development [23]. The exogenous application of BMP2 or BMP4 to embryonic maxillary mesenchymal cells resulted in a significant upregulation of Id1, Id2, and Id3 mRNA [24] and the modulation of Id1, Id2, Id3, as well as Id4 protein levels [25]. BMP2 and BMP4 induced the transcription of Id1, Id2, and Id3 genes in ES cells as well as embryos by promoting the direct binding of the BMP-responsive Smads; Smad1 and Smad5 binding to promoters of these genes [26–28]. This body of evidence suggests important functions of Id proteins during postnatal jaw growth and development.

First, we identified maxillary hypoplasia in Id2 KO mice. We advanced the hypothesis that Id2 abrogation will interfere with the transduction of BMP signaling and, thereby, contributes to maxillary hypoplasia due to abnormal endochondrial ossification in the cranial base synchondrosis during the postnatal growth period. To test our hypothesis, we utilized the Id2 KO mouse model.

Materials and methods

Mice

Id2 mutant mice [14], with a 129/Sv genetic background, were bred under a specific pathogen-free condition and used in this study. All experimental procedures were carried out according to the guidelines for animal experiments regulated by Kyoto University Graduate School of Medicine.

Image analysis of skulls

Neonatal and postnatal mice at the ages of 0, 2, and 12 weeks, respectively, were sacrificed with carbon dioxide gas. The skulls were then analyzed employing an X-ray microtomography method (SMX-100CT-SV3, Shimadzu Co., Kyoto, Japan). The means of the three-dimensional coordinates of these landmarks were used for image analyses of the skull. EDMA was used to measure localized differences between Id2 KO mice and the control group, as described previously [29]. A nonparametric statistical technique was used to evaluate the significance of differences [29].

Analysis of cell proliferation and apoptosis

BrdU (5-Bromo-2′-deoxyuridine, 05650) was injected intraperitoneally at a concentration of 50 μg/g body weight 2 h before sacrifice. Target skeletal tissues were harvested, fixed overnight at 4 °C in a 4% paraformaldehyde solution, and then decalcified in a 0.5 M EDTA solution for 2 weeks. Decalcified samples were embedded in paraffin and sectioned. BrdU-positive cells were detected with BrdU antibody. The rate calculated by expressing the number of BrdU-positive nuclei as a percentage of the total number of nuclei was defined as the proliferation index. Data are presented as the mean ± SD, and further examined with Student's *t*-test. Significance was set at 5%. Apoptotic cells were visualized and identified with the ApopTaq Plus Fluorescein In Situ Apoptosis Detection Kit S7111 (CHEMICON, USA and Canada).

In situ hybridization

In situ hybridization was performed as described previously [30]. Mouse cDNA clones were: Id2 (nt.650-939; NM010496); collagenX (nt.2893-3550; NM009925); and osteopontin (nt.486-844;NM009263).

Immunohistochemistry

Paraffin-embedded sections were subjected to immunostaining with goat polyclonal antibodies directed against Col2 (1:100) (code: 1320-01/SBA), rabbit serum against Col10 (1:200) (code: LB-0092/Lot: 812021/LSL), and primary rabbit antibodies against phosphorylated Smad 1/5/8 (1:100) (Cell Signaling Technology, MA, USA) [31].

Semi-quantitative RT-PCR analysis

Total RNA was cultured with TRIzol (Gibco-BRL, Gaitherburg, MD, USA), according to the manufacturer's instructions, and then quantitated with A260. Oligo(dT)-primed cDNA was prepared with a reverse transcriptase. For the purpose of semiquantitation, 50 ng of cDNA was serially diluted and subjected to PCR amplification with primer pairs. These primer pairs were: Id2, sense, 5′-AGCATCCCCCAGAACAAGAAGGTG-3′ and antisense, 5′-ATCGTCTTGCCCAGGTGTCGTTCT-3′; GAPDH, sense, 5′-CCATCACATCTTCCAGGAG-3′ and antisense, 5′-CCTGCTTCACCACCTTCTTG-3′; BMPR1, sense, 5′-CCTGTTGTTATAGGTCCGTTCTTTG-3′ and antisense, 5′-CGCCATTTACCCATCCATACTT-3′; BMPR2, sense, 5′-CTAACTGGAAATCGGCTGGTG-3′ and antisense, 5′-TGGGTCTCTGCTTCTCTCTGG-3′; Smad1, sense, 5′-AGCCTCTGGAATGCTGTGAGTT-3′ and antisense, 5′-TGGTTGGGGAGTGAGGGTAG-3′; Smad5, sense, 5′-TATGCCAGAACCACAGAAAGGA-3′ and antisense, 5′-ACAGCAAGAGAGGCAGGACTATG-3′; Smad6, sense, 5′-TGCTCAGCAAGGAGCCAGAC-3′ and antisense, 5′-CTGTGGTTGTTGAGTAGGATCTCCA-3′; Smad7, sense, 5′-TGCAGGCTGTCCAGATGCT-3′ and antisense, 5′-CTTGATGGAGAAACCAGGGAAC-3′. All PCR products were examined employing an electrophoretical technique that used 2% agarose gel and ethidium bromide staining. These bands were quantitated with a Bio-image analyzer (Fujix BAS2000, Fuji Photo Film, Tokyo, Japan). All the PCR data were representative from three independent experiments.

Microdissection and organ culture

P7 wild-type mice cranial base structures were dissected in Dulbecco's PBS (pH = 7.4) under a stereomicroscope. The dissected structures were cultured on Nucleopore filters at 37 °C, under a 5% carbon dioxide atmosphere, in a trowel-type organ culture containing BGJb supplemented with 200 ng/ml of BMP-2, BMP-4, and BMP-7 (R&D Systems, MN, USA). The culture medium was renewed every 2 days [31]. After the culture, explants were fixed in a 4% para-formaldehyde and formalin solution, and then processed for histological and immunohistochemical examinations.

Results

Id2 abrogation results in retarded postnatal growth of the maxillofacial complex

Adult Id2-deficient mice showed a shorter maxillofacial profile (Figs. 1A–I). Id2 KO mice present severe clinical phenotypes with

anterior transverse crossbite (Figs. 1A, B and E). The Id2 heterozygous mice showed phenotypically normal profile. We attempted to quantitate the malformation by Euclidean Distance Matrix Analysis (EDMA) to measure and compare the three-dimensional differences between 12-week-old Id2 KO mice, and the control group. We used in these morphometric studies the 89 distances between specific points (Supplemental Figs. 1 and 2). Nasal and frontal bones of Id2 mutants were disproportionally shortened in 32 distances (Fig. 1H). Significant

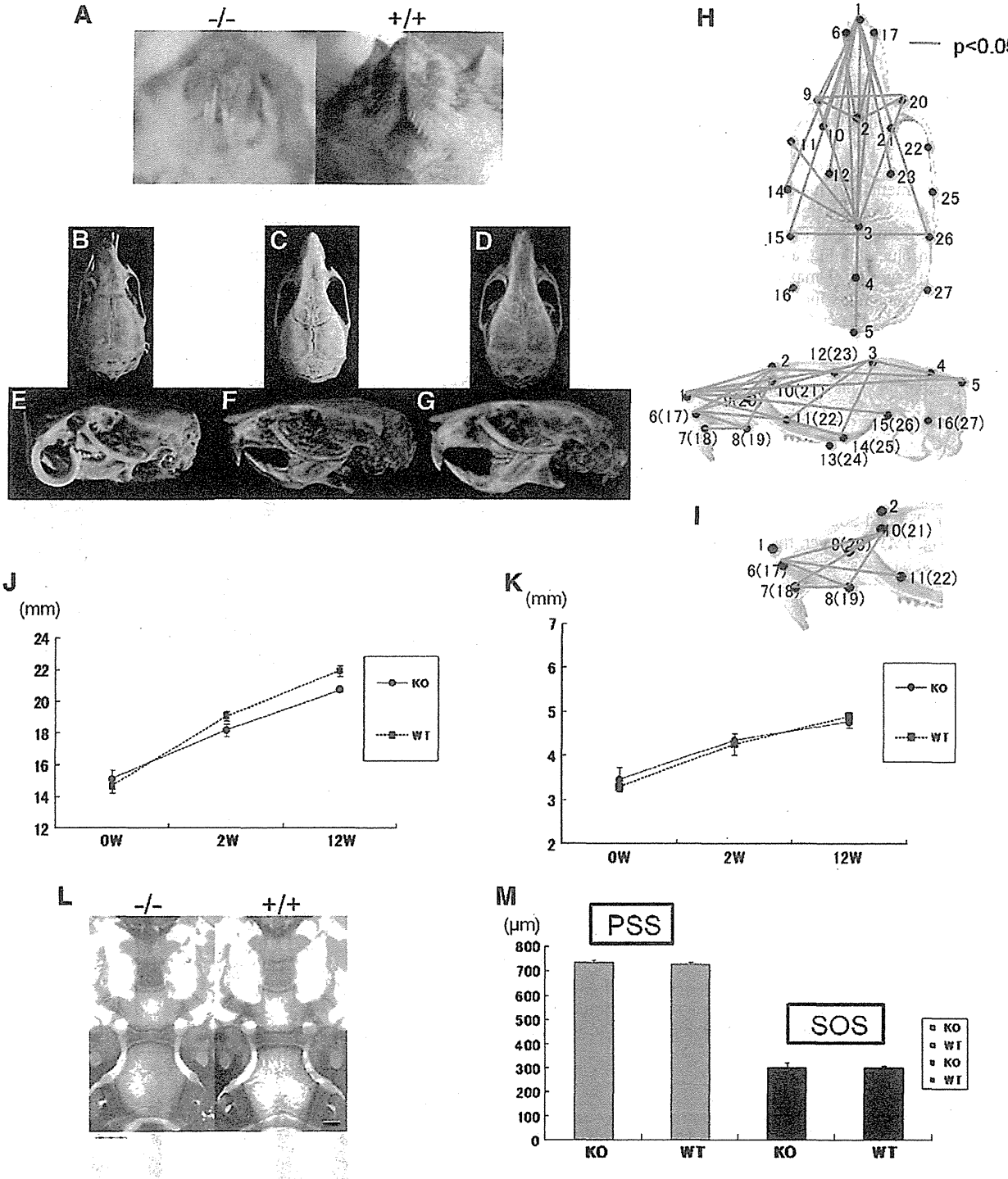

Fig. 1. The shorter maxillofacial profile in adult Id2-deficient mice. Comparison of the Id2 KO and control groups in week 12. (A) Facial differences between Id2 KO (right panel) and the control (left panel). Superior view of adult mouse skulls: Id2 KO (severe case) (B), Id2 KO (mild case) (C), and the control (D). Lateral view of adult mouse skulls: Id2 KO (severe case) (E), Id2 KO (mild case) (F), and the control (G). (H) Measurement of the cranial dimensions. Landmarks used for cranial measurements were based on those used by Arron JR et al. (Supplemental Fig. 1) [29]. The red lines indicate significantly different distances between Id2 KO and the wild-type. $p<0.05$ using Student's *t*-test. (I) Detailed measurement of the premaxilla and maxilla. The red lines indicate significantly different distances between Id2 KO and the wild-type. $p<0.05$ using Student's *t*-test. The longitudinal distance between the nasal and intersection of the interparietal and occipital bones at the midline (J), and the width of the bilateral frontal-squamosal intersection at the temporal crest, with age (K). (L) Alizarin red and Alcian blue staining did not differentiate the Id2 KO from the control skull base. (M) The length of the presphenoid synchondrosis (gray bar) and spheno-occipital synchondrosis (black bar) did not differ between the two groups ($n=3$). All error bars indicated one standard deviation of uncertainty.

differences were noted in the distances between the (a) nasal and intersection of interparietal and occipital bones at the midline (1–5), (b) nasal and frontal-squamosal intersection at the temporal crest (1-12(23)), (c) nasal and intersection of the frontal process of the maxilla with frontal and lacrimal bones(1-10(21)), (d) bregma and anterior-most point at the intersection of premaxillae and nasal bones(3-6(17)), and (e) bregma and anterior notch on the frontal process lateral to the infraorbital fissure(3-9(20)). In summary, landmarks in the premaxilla and maxilla of Id2 mutant mice were influenced in what appeared to be a longitudinal direction (Fig. 1I). Importantly, there were no differences in the skull width between KO and WT mice after birth were observed (Figs. 1H and K). The difference in the longitudinal diameter between the two groups increased with age (Fig. 1J). To explore the relationship between embryonic development and maxillary hypoplasia in Id2-deficient mice, newborn pups were examined. Newborn Id2-deficient mice were not different from their WT counterparts in appearance, Alizarin red and Alcian blue staining, and EDMA (Fig. 1L). These results indicated that the severity of maxillary hypoplasia or dysmorphogenesis in Id2-deficient mice increased with postnatal growth and development. Curiously, the cranio-maxillofacial region of newborn mice was found to be essentially identical between WT and mutant.

Abnormal differentiation of the synchondrosal growth plate is caused by Id2 abrogation

PSS and SOS are important growth centers of the cranio-maxillofacial skeleton, and appear to influence the temporal and positional cues for the growth and development of the maxilla [7,32,33]. There were no differences in PSS and SOS between newborn as well as adult KO and WT mice (Fig. 1M). However, the zone of hypertrophic chondrocytes in the cranial base was narrower in the 2-week-old Id2 KO than the WT group (Figs. 2C and D). To assess the hypertrophy of chondrocytes, type X collagen (a molecular marker of the hypertrophic zone) and osteopontin (a molecular marker of the calcified zone) expressions were examined. Similar to the histological results, the distribution of type X collagen was down-regulated in Id2-deficient mice, whereas osteopontin was similarly distributed in the KO and WT tissue samples (Figs. 2G–J). The total length of SOS in Id2-deficient mice was reduced when compared to WT (Fig. 2K). These results suggest that abnormal postnatal growth of the cranial base in mutant Id2 mice resulted from the disturbed hypertrophy of chondrocytes in synchondroses.

Reduced proliferative activity of synchondrosal chondrocytes in Id2 KO mice

The proliferative activity of chondrocytes in synchondroses of the cranial base was examined employing a BrdU labeling method. The number of dividing cells in the proliferative zone of 2-week-old mutant PSS and SOS significantly decreased (Figs. 3A: a–d and B). Proliferation was reduced in the nasal septal cartilage of KO mice (Fig. 3A: e–h). Apoptosis within synchondroses was examined with a TUNEL method. Both mutant and control groups failed to display the apoptosis of chondrocytes (Fig. 3C).

Expression of Id2 in the synchondrosis of the cranial base

The expression of Id2 mRNA in the synchondrosis of the cranial base was evaluated using a semi-quantitative RT-PCR method. Id2

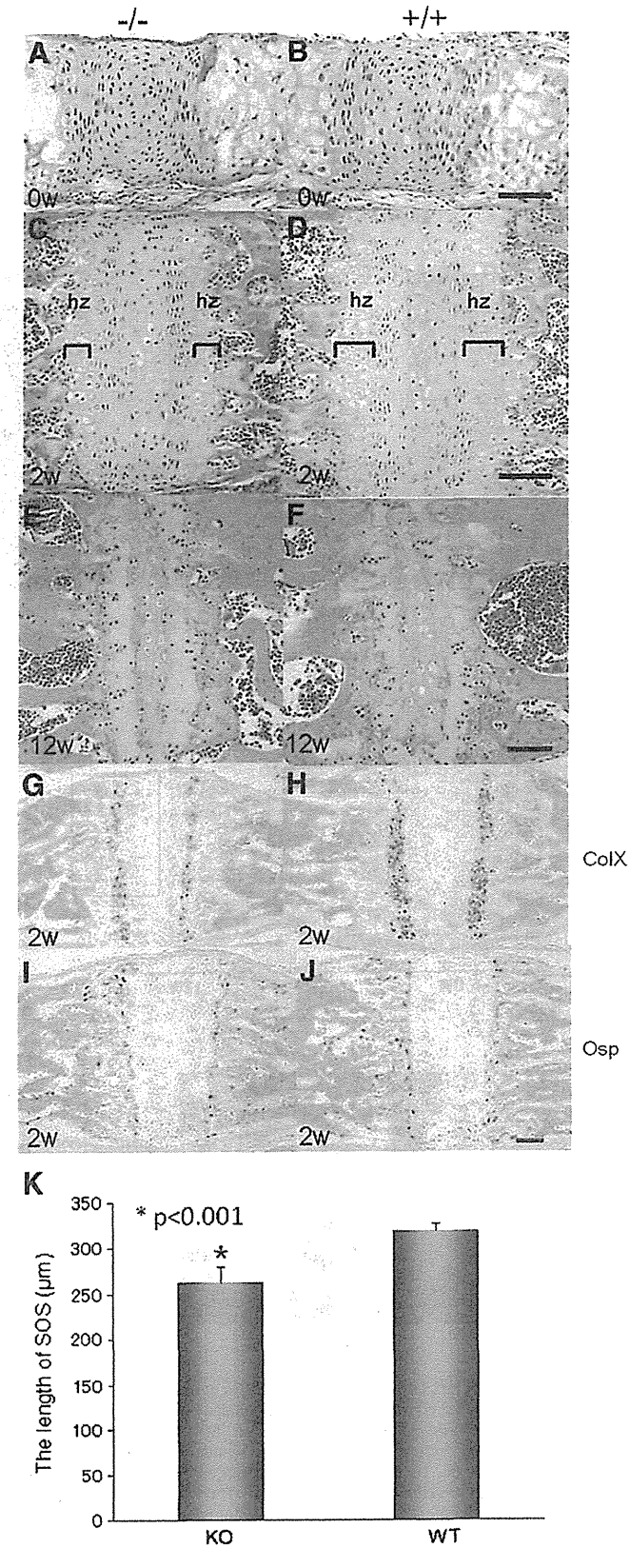

Fig. 2. Abnormal differentiation of the synchondrosal growth plate caused by the absence of Id2. In week 0, the Id2 KO and control groups did not show a difference in SOS (A and B). In week 2, the two groups revealed a difference in hypertrophic chondrocytes of SOS (C and D). In week 12, the two groups showed no difference in SOS (E and F). In week 2, the expression pattern of type X collagen in the two groups showed a difference of hypertrophic chondrocytes in SOS (G and H) visualized by in situ hybridization. In week 2, expression patterns of osteopontin in the two groups did not differ in SOS (I and J) visualized by in situ hybridization. (hypertrophic zone (hz): bracket. Scale bar: 100 μm). (K) The length of the SOS in transverse sections of Id2-deficient (left bar) as well as wild-type (right bar) mice is shown as an average length. Five sections were prepared from five different mice. All error bars are standard deviations of uncertainty. $p<0.001$ by Student's *t*-test.

transcript expression in the cranial base was significant in postnatal facial development, and kept the same level in 2-week, 4-week, 6-week or 12-week-old after birth (Fig. 4A: a). Id2 is also expressed in many adult tissues including spleen, brain, liver, bone marrow, heart and kidney (Fig. 4A: b). Analyses of in situ hybridization showed that Id2 was ubiquitously expressed in all portions of synchondroses, including the proliferating and hypertrophic zones (Fig. 4B). This was interpreted to mean that Id2 expression in synchondroses was detected but not localized to a specific region.

Suppressed chondrocyte proliferation and differentiation on exposure to exogenous BMPs in the cranial base of Id2 KO mice in vitro

Id expression is regulated by a BMP-Smad signaling pathway. We assayed the functions of BMP2, BMP4, and BMP7 in the cranial base in vitro. The cranial bases were isolated from 7-day-old mice, which referred to the postnatal growing and developmental stage, and divided into three groups: treated with exogenous BMP2 (200 ng/ml), BMP4 (200 ng/ml), or BMP7 (200 ng/ml) every 2 days for three continuous cycles (total: 6 days) (Fig. 5A: a–h). In the BMP2 and BMP4 groups, an additional increase in the PSS length of Id2 WT cranial bases was observed (Figs. 5A: d and f and B). Histochemical analyses of type II and X collagen were conducted. In the presence of exogenous BMP2, the degree of chondrocyte hypertrophy from Id2 WT cranial bases increased (Figs. 5D and F: d–f). The application of BMP2 failed to cause a difference in the degree of chondrocyte hypertrophy between Id2 KO and control cranial bases (Figs. 5C and E: d–f). The degrees of chondrocyte hypertrophy adjacent to the bone and ectopic hypertrophy surrounding the central reserve zone of synchondroses increased in the Id2 WT group receiving exogenous BMP4 (200 ng/ml) (Figs. 5D and F: g–i). The increase of the hypertrophy due to the application of BMP4 did not differ between Id2 KO and control cranial bases (Figs. 5C and E: g–i). In the BMP7 group, the amount of proliferative chondrocytes from Id2 WT cranial bases increased (Figs. 5D and F: j–l). No other differences between Id2 KO and control cranial bases were identified in the BMP7 group

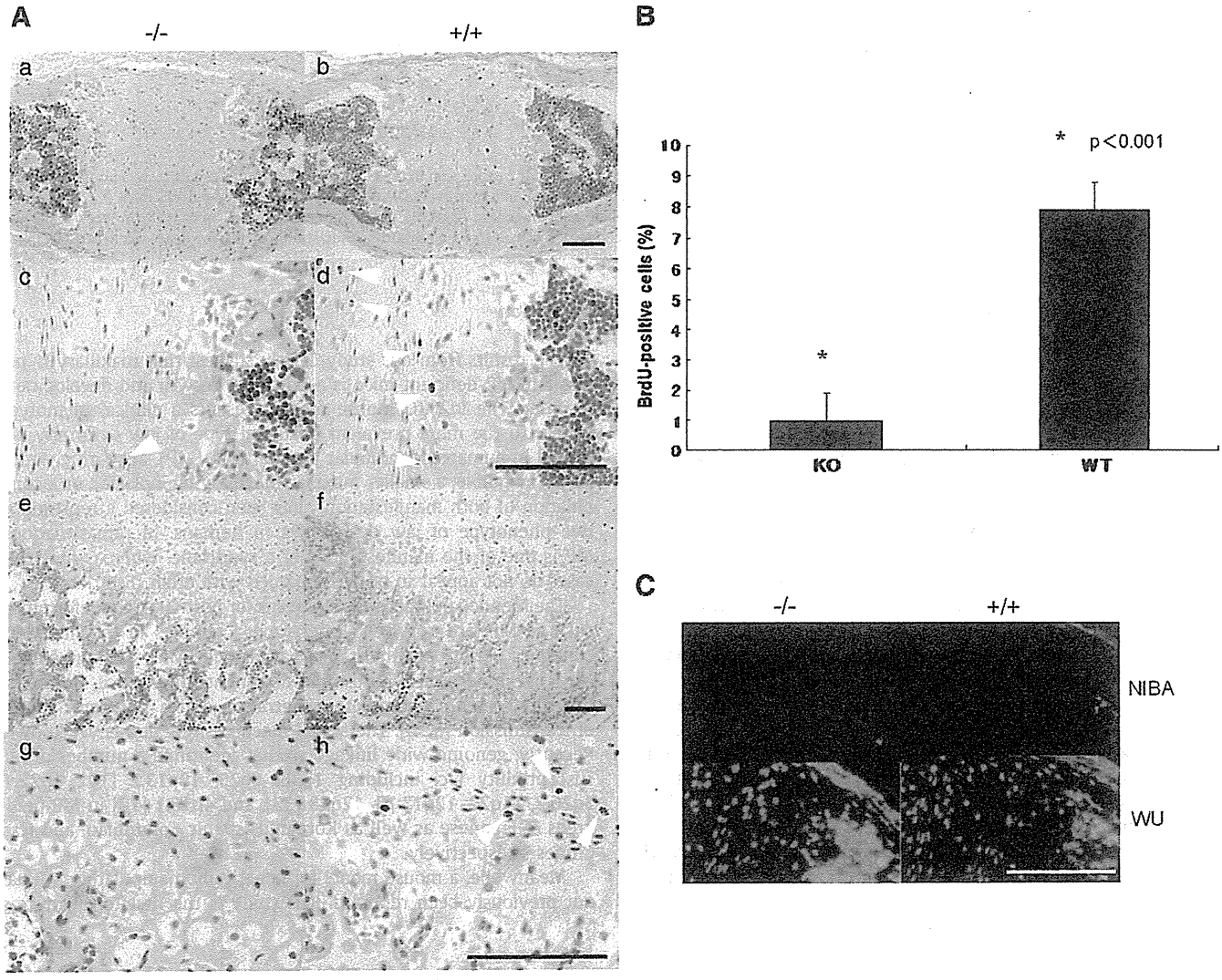

Fig. 3. Reduced proliferative activity of synchondrosal chondrocytes in Id2-deficient mice. (A) The reduction of chondrocyte proliferation in Id2 KO PSS and NSC. Sagittal view of 2-week-old PSS in the Id2 KO and control cranial base (a–d); lower (a, b) and higher (c, d) magnification. The white arrow-head indicates BrdU-positive cells (c, d). Sagittal view of 2-week-old NSC in the Id2 KO and control (e–h); lower (e, f) and higher (g, h) magnification. The white arrowhead indicates BrdU-positive cells (h). The number of BrdU-positive cells. (B) The proliferative rate of the Id2 KO (left bar) and control (right bar) PSS chondrocytes is shown as an average percent of BrdU-positive cells relative to the total cell count. Three sections were prepared from three different mice. All error bars are standard deviations of uncertainty. $p<0.05$ by Student's t-test. (C) No apoptotic cells in Id2 KO presphenoid and spheno-occipital synchondrosis. Sagittal view of 2-week-old presphenoid synchondrosis in the Id2 KO and control cranial base (a–d); NIBA (a, b) and WU (c, d) images. All scale bars: 100 μm.

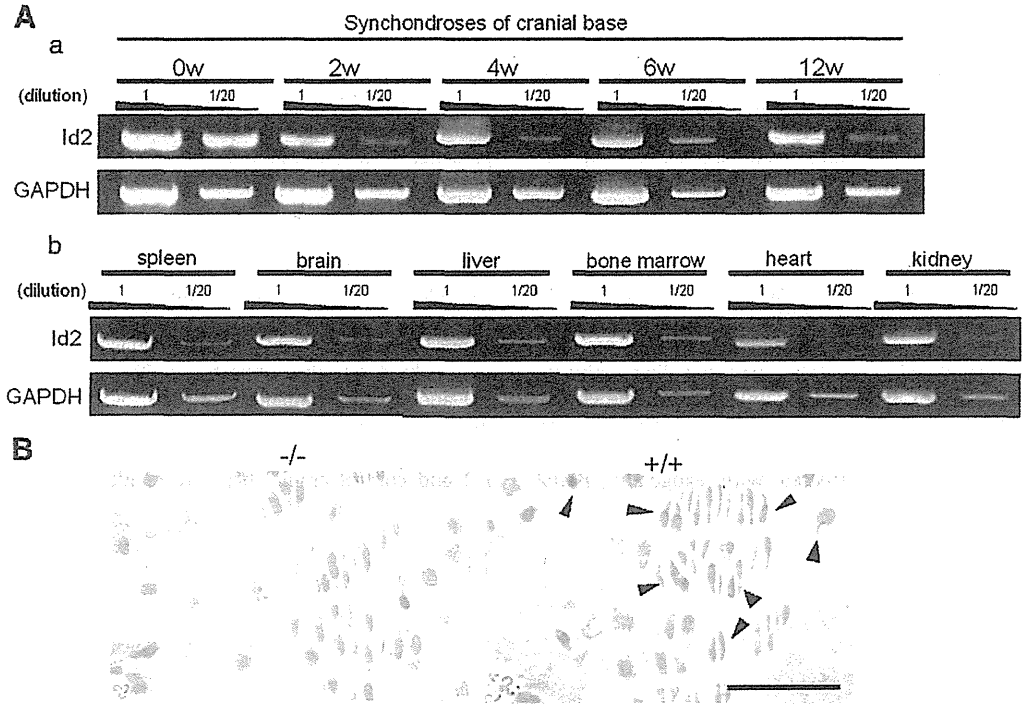

Fig. 4. Expression of Id2 in the cranial base synchondrosis. (A) Semi-quantitative RT-RCR analysis of Id2 expression in the cranial base synchondrosis. RNA was purified from the cranial base synchondrosis of 0-, 2-, 4-, 6-, and 12-week-old WT mice (a), and spleen, brain, liver, bone marrow, heart and kidney of 12-week-old WT mice (b). RT products were twentyfold serially diluted and subjected to PCR. Reduced glyceraldehyde-phosphate dehydrogenase (GAPDH) was used as an internal control. (B) In week 2, Id2 was detected in the cranial base synchondrosis, especially in proliferative and hypertrophic chondrocytes, using section in situ hybridization (black arrowhead). Scale bar: 50 μm.

(Figs. 5C and E: j–l). Exogenous BMPs enhanced chondrocyte differentiation and proliferation in the WT but not in the mutant model.

Id2 regulates BMP signaling in synchondrosis of the cranial base through inhibiting Smad7 expression

In order to identify the downstream target gene of Id2 in synchondrosis of the cranial base, we evaluated levels of expression of BMP signaling molecules including BMPR-I, BMPR-II, and several different kind of Smads. The expression of mRNAs in the synchondrosis of the cranial base within Id2 WT and KO mice was evaluated using a semi-quantitative RT-PCR method. We discovered more than five-fold up-regulation of the Smad7 transcripts, which belonged to inhibitory Smad, within the Id2-deficient mice samples (Fig. 6A). Furthermore, in order to assess whether the up-regulation of Smad7 in Id2-deficient mice is attributable to the inhibition of BMP signaling, the phosphorylation of Smad 1,5,8 was examined. Compared with the wild type, Id2-deficient mice exhibited the decreased phosphorylation of Smad 1,5,8-positive cells in chondrocytes within the synchondrosis of the cranial base (Figs. 6B and C). These data indicate Id2 controls chondrogenesis during early postnatal maxillary and mandibular growth and development by acting downstream of BMP signaling to regulate chondrocyte proliferation and differentiation and by enhancing BMP signaling through inhibiting Smad7 expression (Fig. 7).

Discussion

The results from our study clearly suggest that maxillary hypoplasia in Id2-deficient mice is a postnatal growth and development disorder. The Id2 KO mouse model presents a clinical phenotype similar to the more prevalent postnatal type of jaw deformity observed in humans. Mandibular prognathism (MP), appearing with a larger mandible, a smaller maxilla (maxillary hypoplasia), or a combination of both manifestations, has been considered a representative phenotype of jaw deformities in humans. In rare situations, MP is one of the manifestations of a syndrome, whereas most MP cases do not appear to be accompanied with other disorders.

The Mendelian inheritance patterns for postnatal jaw deformities, such as MP, are not well understood. Examples in the literature contain a variety of inheritance patterns for MP — an autosomal-recessive inheritance, autosomal-dominant inheritance, dominant inheritance with incomplete penetrance, and a polygenic model of transmission [9,34]. The actual mechanism is not as yet known. Recently, genome-wide linkage studies identified a number of MP susceptibility loci including 1p36, 6q25, 19p13.2 [10], 1p22.1, 3q26.2, 11q22, 12q13.13, 12q23 [35], and 4p16.1 [10] in MP pedigrees of Japanese as well as Korean, Hispanic Colombian, and Han Chinese, respectively.

Meanwhile, a mouse model for genetically manipulating MP has not previously been reported. Our study is the first to illustrate a

Fig. 5. BMP-2, -4, and -7 promoted chondrocyte hypertrophy and proliferation in synchondroses of the cranial base in WT but not in Id2 KO mice in vitro. (A) On postnatal day 7, cranial base explants cultured under serum-free conditions to induce in vitro development were exposed to 200 ng/ml of BMP2 (c and d), BMP4 (e and f), and BMP7 (g and h). BMP2 and BMP4 enhanced chondrocyte hypertrophy in the control (white arrowheads). (B) The length of the PSS of Id2-deficient (gray bar) as well as wild-type (black bar) mice on day 6 of organ culture is shown as an average length. Each average length of the PSS was calculated from three different explants. All error bars are standard deviations of uncertainty. $p<0.05$ by Student's *t*-test. Low magnification of Id2-deficient (C) and wild-type mice (D). High magnification of Id2-deficient (E) and wild-type mice (F). Midsagittal sections of PSS were stained with H&E (C–F: a, d, g, and j), immunostained for type II collagen (C–F: b, e, h, and k), or type X collagen (C–F: c, f, i, and l). The section was respectively, control (C–F: a–c) and exposed to BMP2 (C–F: d–f), BMP4 (C–F: g–i), and BMP7 (C–F: j–l). BMP2 and BMP4 enhanced chondrocyte hypertrophy (E: d–i and F: d–i). BMP7 enhanced chondrocyte proliferation (F: j–l) (hypertrophic zone (hz): bracket; proliferative zone (pz): bracket; ectopic hypertrophy: asterisks). All scale bars: 100 μm.

mouse model for postnatal jaw deformities. This model provides an opportunity to explore the molecular mechanisms underlying jaw deformity, with particular emphasis on maxillary hypoplasia.

The synchondrosis of the cranial base is an important growth center of the craniofacial skeleton, and provides an anatomical, developmental linkage between the cranial vault and formation of

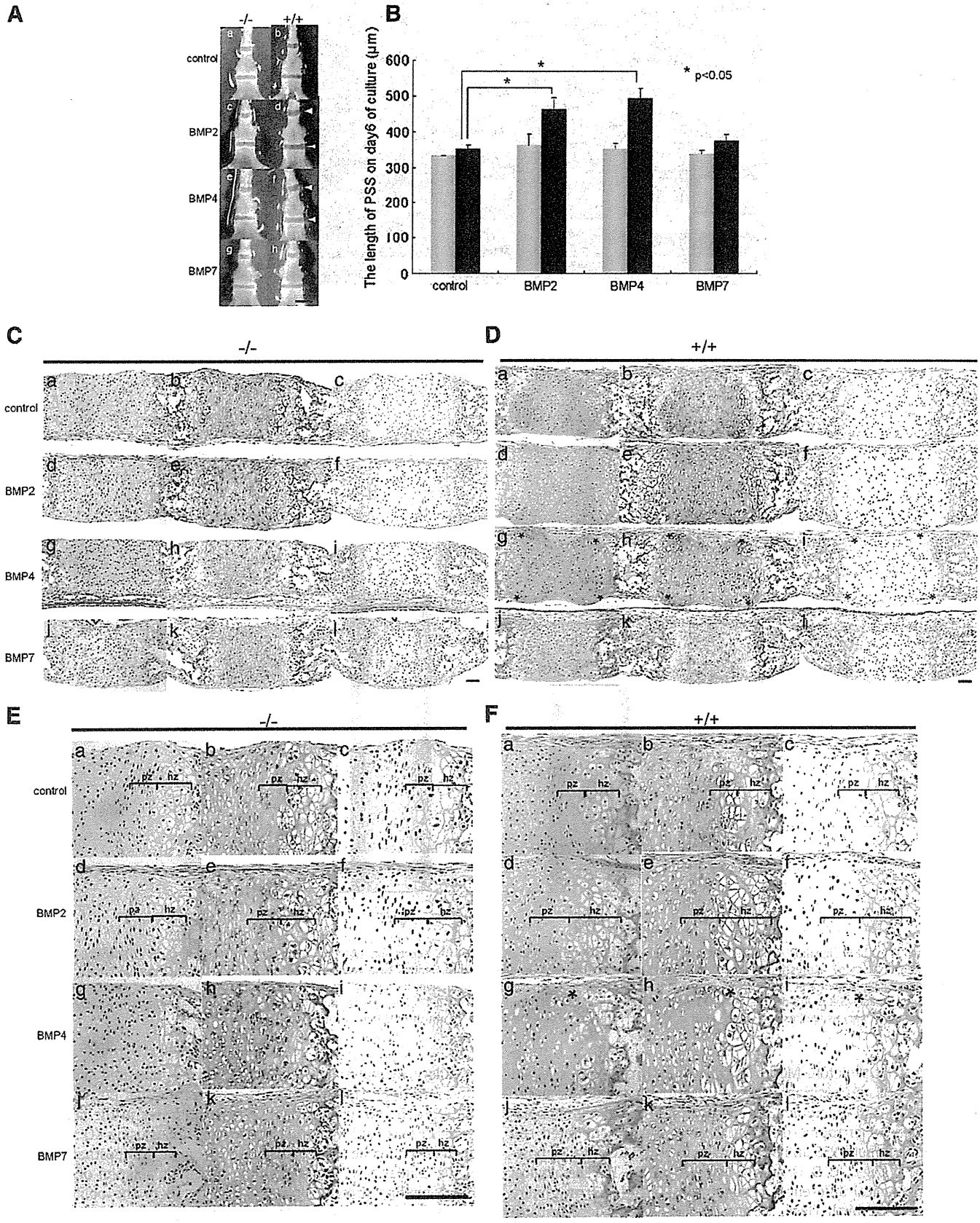

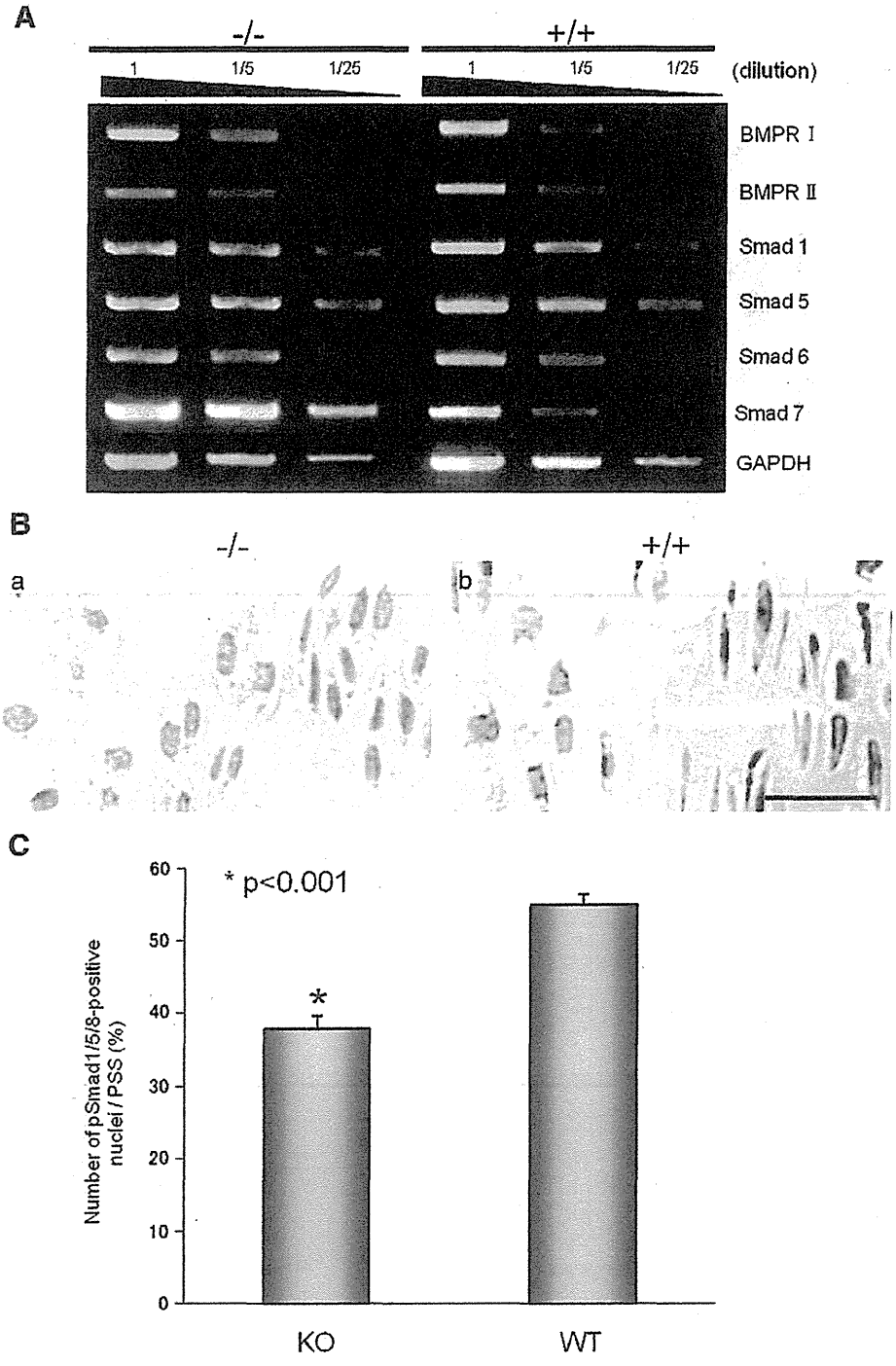

Fig. 6. Id2 regulates BMP signaling in synchondrosis of the cranial base through inhibiting Smad7 expression. (A) Semi-quantitative RT-PCR analysis of BMPRI BMPRII Smad1, Smad5, Smad6, and Smad7 expression in cranial base synchondrosis. RNA was purified from the cranial base synchondrosis of 2-week-old Id2 KO and WT mice. RT products were fivefold serially diluted and subjected to PCR. Reduced glyceraldehyde-phosphate dehydrogenase (GAPDH) was used as an internal control. (B) Immunolocalization of phosphorylated Smad 1/5/8 in Id2-deficient (a) and wild-type (b) mice. (C) The number of pSmad 1/5/8 – positive nuclei in PSS per section was counted in transverse sections of Id2-deficient (left bar) as well as wild-type (right bar) mice. Three sections were prepared from three different mice.

the craniofacial skeleton. Moreover, this growth center is relevant to the temporal and positional cues for the growth and development of the maxilla and mandible [32]. In addition to maxillary hypoplasia, retarded hypertrophic differentiation as well as inhibited cell proliferation in both PSS and SOS was found in Id2 KO mice in postnatal week 2 (Figs. 2C, D, G, and H; Figs. 3A and B). The histological and morphological differences between Id2 KO and WT mice were not observed at birth (Figs. 1L and M; Fig. 2A). The severity of maxillary hypoplasia in Id2-deficient mice increased with growth after birth (Fig. 1J). These results demonstrate that postnatal abnormal growth and development of synchondroses in the cranial base result in maxillary hypoplasia. Previous studies using KO mice identified several genes that regulated embryonic and postnatal growth of the cranial base. As an example, a genetic ablation of the latent TGF-β-binding protein (*Ltbp-3*) contributed to the obliteration of cranial base synchondrosis and a dome-shaped skull [36]. Premature

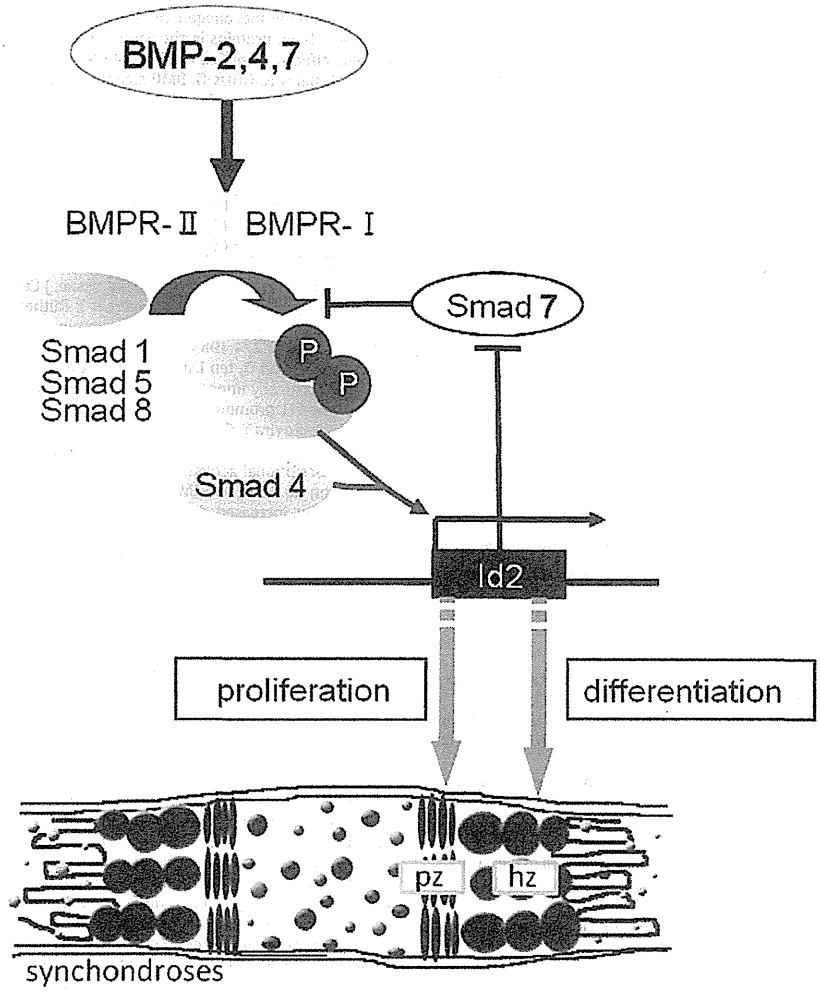

Fig. 7. Diagrammatic representation of the function of Id2 acting downstream of BMP signaling through inhibiting Smad7 in cranial base synchondroses during the postnatal growth period. Inhibition of Smad7 function by Id2 proteins. In general, Smad7, one of the inhibitory Smads, interferes with the recruitment and phosphorylation of R-Smads. Id2 inhibits the functions of Smad7. Id2 exists in proliferating and hypertrophic chondrocytes at the synchondrosis of the cranial base. Id2 acts on receptors on hypertrophic chondrocytes to keep them hypertrophic and, thereby, promotes the production of BMP2 and BMP4 through Smad. Id2 acts on receptors on proliferating chondrocytes to keep them proliferating and, thereby, promotes the production of BMP7 through Smad.

hypertrophy of the synchondrosis was found in *Ltbp-3* knockout mice [36]. A premature closure of the cranial base PSS, as well as SOS and accompanying craniofacial malformation, was observed in the conditional KO mouse strains of polycystin-1 (*Pkd-1*) [12]. Even though these studies did not report whether or not the mutant mice sustained jaw deformities, their results clearly demonstrated a link between craniofacial deformity and impaired synchondroses of the cranial base. Furthermore, cranial malformation of these mutant mice seemed to appear before birth, since the abnormality of synchondroses has been observed during embryonic development.

Studies have reported that the chondrogenic potential of cells derived from developing mouse craniofacial tissues was regulated via the alteration of Id protein functions through over-expression of the bHLH factor [37]. Mouse trunk neural crest cells, which do not contribute skeletal derivatives, can undergo chondrogenesis and the expression of Id2 is up-regulating by FGF2 treatment in vitro [38]. Proper expression of Id2 is important to chondrogenic differentiation of ATDC cells [39]. It was reported that Id2 was expressed in proliferating chondrocytes of growth plate at E16.5 mouse embryo by immunohistochemistry [39]. Furthermore, the expression of Id2 was showed in proliferating chondrocytes of the developing digits in chick embryo, and expression of Id2 in vivo and in vitro was up-regulated by BMP7 supplement [40]. Indeed, we also detect the Id2 expression in proliferating chondrocytes of the synchondrosis of the cranial base at postnatal developing stage (Fig. 4B). Although these results suggest that Id2 are critical controls for chondrogenesis and osteogenesis in vitro systems and are expressed in chondrocytes in vivo, the physiological function for Ids has not been demonstrated. Our report is the first to demonstrate the involvement of the Id2 gene in chondrocyte differentiation, chondrocyte proliferation, and endochondral ossification in vivo. The Id2 knock-out mouse model showed the inhibition of cell proliferation and hypertrophic differentiation of chondrocytes in the cranial base synchondrosis. This mouse model provides a unique opportunity to explain the physiological activity of Id2 transcriptional controls and its role in postnatal jaw deformities.

Inhibitory Smads including Smad6 and Smad7 inhibit the phosphorylation of receptor-regulated Smads (R-Smad) [41]. Smad6 inhibits BMP signaling, whereas Smad7 inhibits both TGF-β and BMP signaling [42]. Smad7 is expressed in growth plate cartilage [43]. In vitro studies using cell culture systems or the organ culture of mandibular explants have shown that Smad7 inhibits chondrocyte differentiation and/or proliferation induced by TGF-β [44,45] and BMP [46,47]. These in vitro studies demonstrated the down-regulation of R-Smad activation by Smad7 in chondrocytes. Recently, Smad7 was found to inhibit chondrocyte differentiation at multiple steps during

endochondral bone formation using conditional transgenic mice [48]. Furthermore, BMP-induced cartilaginous nodule formation was down-regulated by the overexpression of Smad7, but not Smad6 [48]. Indeed, in our experiment, the up-regulation of Smad7 as a result of Id2 abrogation led to the inhibition of chondrocyte proliferation and differentiation.

In summary, the present study demonstrated that Id2 functions by acting downstream of BMP signaling to regulate cartilage formation during postnatal growth and development by enhancing BMP signals through inhibiting Smad7 expression. These interactions contribute to endochondral ossification in the cranial base synchondrosis during the growth period.

Supplementary materials related to this article can be found online at doi:10.1016/j.bone.2011.09.049.

Acknowledgments

This study was supported by a Grant-in-Aid for Young Scientists (B) from the Japanese Society for the Promotion of Science. We thank the all members of Translation Research Center (Kyoto University Hospital) for the great technical support and discussions in this study.

References

[1] Proffit William R, White Raymond P, Sarver Jr David M, editors. Contemporary treatment of dentofacial deformity. Philadelphia, USA: Mosby; 2003.
[2] Susami R, Asai Y, Hirose K, Hosoi T, Hayashi I. Prevalence of malocclusion in Japanese school children. 4. The frequency of mandibular overjet. Nippon Kyosei Shika Gakkai Zasshi 1972;31:319–24.
[3] Tang EL. The prevalence of malocclusion amongst Hong Kong male dental students. Br J Orthod 1994;21:57–63.
[4] Allwright WC, Bundred WH. A survey of handicapping dentofacial anomalies among Chinese in Hong Kong. Int Dent J 1964;14:505–19.
[5] Emirich RE, Brodie AG, Blayney JR. Prevalence of class I, class II, class III malocclusions (Angle) in an urban population; an epidemiological study. J Dent Res 1965;44: 947–53.
[6] Xue F, Wong RW, Rabie AB. Genes, genetics, and Class III malocclusion. Orthod Craniofac Res 2010;13:69–74.
[7] Singh GD. Morphologic determinants in the etiology of class III malocclusions: a review. Clin Anat 1999;12:382–405.
[8] Li Q, Zhang F, Li X, Chen F. Genome scan for locus involved in mandibular prognathism in pedigrees from China. PLoS One 2010;5.
[9] Cruz RM, Krieger H, Ferreira R, Mah J, Hartsfield Jr J, Oliveira S. Major gene and multifactorial inheritance of mandibular prognathism. Am J Med Genet A 2008;146A:71–7.
[10] Yamaguchi T, Park SB, Narita A, Maki K, Inoue I. Genome-wide linkage analysis of mandibular prognathism in Korean and Japanese patients. J Dent Res 2005;84:255–9.
[11] Ranly DM. Craniofacial growth. Dent Clin North Am 2000;44:457–70.
[12] Kolpakova-Hart E, McBratney-Owen B, Hou B, Fukai N, Nicolae C, Zhou J, et al. Growth of cranial synchondroses and sutures requires polycystin-1. Dev Biol 2008;321:407–19.
[13] Sugai M, Gonda H, Nambu Y, Yokota Y, Shimizu A. Role of Id proteins in B lymphocyte activation: new insights from knockout mouse studies. J Mol Med 2004;82: 592–9.
[14] Yokota Y, Mansouri A, Mori S, Sugawara S, Adachi S, Nishikawa S, et al. Development of peripheral lymphoid organs and natural killer cells depends on the helix–loop–helix inhibitor Id2. Nature 1999;397:702–6.
[15] Sugai M, Gonda H, Kusunoki T, Katakai T, Yokota Y, Shimizu A. Essential role of Id2 in negative regulation of IgE class switching. Nat Immunol 2003;4:25–30.
[16] Norton JD. ID helix–loop–helix proteins in cell growth, differentiation and tumorigenesis. J Cell Sci 2000;113:3897–905.
[17] Iavarone A, Garg P, Lasorella A, Hsu J, Israel MA. The helix–loop–helix protein Id-2 enhances cell proliferation and binds to the retinoblastoma protein. Genes Dev 1994;8:1270–84.
[18] Atherton GT, Travers H, Deed R, Norton JD. Regulation of cell differentiation in C2C12 myoblasts by the Id3 helix–loop–helix protein. Cell Growth Differ 1996;7:1059–66.
[19] Lyden D, Young AZ, Zagzag D, Yan W, Gerald W, O'Reilly R, et al. Id1 and Id3 are required for neurogenesis, angiogenesis and vascularization of tumour xenografts. Nature 1999;401:670–7.
[20] Ying QL, Nichols J, Chambers I, Smith A. BMP induction of Id proteins suppresses differentiation and sustains embryonic stem cell self-renewal in collaboration with STAT3. Cell 2003;115:281–92.
[21] Abe J. Bone morphogenetic protein (BMP) family, SMAD signaling and Id helix–loop–helix proteins in the vasculature: the continuous mystery of BMPs pleotropic effects. J Mol Cell Cardiol 2006;41:4–7.
[22] Hoffmann A, Gross G. BMP signaling pathways in cartilage and bone formation. Crit Rev Eukaryot Gene Expr 2001;11:23–45.
[23] Takahashi K, Nuckolls GH, Tanaka O, Semba I, Takahashi I, Dashner R, et al. Adenovirus-mediated ectopic expression of Msx2 in even-numbered rhombomeres induces apoptotic elimination of cranial neural crest cells in ovo. Development 1998;125:1627–35.
[24] Mukhopadhyay P, Singh S, Greene RM, Pisano MM. Molecular fingerprinting of BMP2- and BMP4-treated embryonic maxillary mesenchymal cells. Orthod Craniofac Res 2006;9:93–110.
[25] Mukhopadhyay P, Webb CL, Warner DR, Greene RM, Pisano MM. BMP signaling dynamics in embryonic orofacial tissue. J Cell Physiol 2008;216:771–9.
[26] Hollnagel A, Oehlmann V, Heymer J, Rüther U, Nordheim A. Id genes are direct targets of bone morphogenetic protein induction in embryonic stem cells. J Biol Chem 1999;274:19838–45.
[27] Korchynskyi O, ten Dijke P. Identification and functional characterization of distinct critically important bone morphogenetic protein-specific response elements in the Id1 promoter. J Biol Chem 2002;277:4883–91.
[28] López-Rovira T, Chalaux E, Massagué J, Rosa JL, Ventura F. Direct binding of Smad1 and Smad4 to two distinct motifs mediates bone morphogenetic protein-specific transcriptional activation of Id1 gene. J Biol Chem 2002;277:3176–85.
[29] Arron JR, Winslow MM, Polleri A, Chang CP, Wu H, Gao X, et al. NFAT dysregulation by increased dosage of DSCR1 and DYRK1A on chromosome 21. Nature 2006;441:595–600.
[30] Murashima-Suginami A, Takahashi K, Kawabata T, Sakata T, Tsukamoto H, Sugai M, et al. Rudiment incisors survive and erupt as supernumerary teeth as a result of USAG-1 abrogation. Biochem Biophys Res Commun 2007;359:549–55.
[31] Murashima-Suginami A, Takahashi K, Sakata T, Tsukamoto H, Sugai M, Yanagita M, et al. Enhanced BMP signaling results in supernumerary tooth formation in USAG-1 deficient mouse. Biochem Biophys Res Commun 2008;369:1012–6.
[32] Bjork A. Cranial base development. Am J Orthod 1995;41:198–225.
[33] Lei WY, Wong RW, Rabie AB. Factors regulating endochondral ossification in the spheno-occipital synchondrosis. Angle Orthod 2008;78:215–20.
[34] Wolff G, Wienker TF, Sander H. On the genetics of mandibular prognathism: analysis of large European noble families. J Med Genet 1993;30:112–6.
[35] Frazier-Bowers S, Rincon-Rodriguez R, Zhou J, Alexander K, Lange E. Evidence of linkage in a Hispanic cohort with a Class III dentofacial phenotype. J Dent Res 2009;88:56–60.
[36] Dabovic B, Chen Y, Colarossi C, Obata H, Zambuto L, Perle MA, et al. Bone abnormalities in latent TGF-[beta] binding protein (Ltbp)-3-null mice indicate a role for Ltbp-3 in modulating TGF-[beta] bioavailability. J Cell Biol 2002;156:227–32.
[37] Mukhopadhyay P, Rezzoug F, Webb CL, Pisano MM, Greene RM. Suppression of chondrogenesis by Id helix–loop–helix proteins in murine embryonic orofacial tissue. Differentiation 2009;77:462–72.
[38] Ido A, Ito K. Expression of chondrogenic potential of mouse trunk neural crest cells by FGF2 treatment. Dev Dyn 2006;235:361–7.
[39] Yang L, Ma X, Lyone A, Zou J, Blackburn ML, Pan J, et al. Proper expression of helix–loop–helix protein Id2 is important to chondrogenic differentiation of ATDC5 cells. Biochem J 2009;419:635–43.
[40] Lorda-Diez CI, Torre-Pérez N, García-Porrero JA, Hurle JM, Montero JA. Expression of Id2 in the developing limb is associated with zones of active BMP signaling and marks the regions of growth and differentiation of the developing digits. Int J Dev Biol 2009;53:1495–502.
[41] Massagué J, Seoane J, Wotton D. Smad transcription factors. Genes Dev 2005;19: 2783–810.
[42] Goto K, Kamiya Y, Imamura T, Miyazono K, Miyazawa K. Selective inhibitory effects of Smad6 on bone morphogenetic protein type I receptors. J Biol Chem 2007;282:20603–11.
[43] Sakou T, Onishi T, Yamamoto T, Nagamine T, Sampath T, Ten Dijke P. Localization of Smads, the TGF-beta family intracellular signaling components during endochondral ossification. J Bone Miner Res 1999;14:1145–52.
[44] Ito Y, Bringas Jr P, Mogharei A, Zhao J, Deng C, Chai Y. Receptor-regulated and inhibitory Smads are critical in regulating transforming growth factor beta-mediated Meckel's cartilage development. Dev Dyn 2002;224:69–78.
[45] Scharstuhl A, Diepens R, Lensen J, Vitters E, van Beuningen H, van der Kraan P, et al. Adenoviral overexpression of Smad-7 and Smad-6 differentially regulates TGF-beta-mediated chondrocyte proliferation and proteoglycan synthesis. Osteoarthritis Cartilage 2003;11:773–82.
[46] Fujii M, Takeda K, Imamura T, Aoki H, Sampath TK, Enomoto S, et al. Roles of bone morphogenetic protein type I receptors and Smad proteins in osteoblast and chondroblast differentiation. Mol Biol Cell 1999;10:3801–13.
[47] Valcourt U, Gouttenoire J, Moustakas A, Herbage D, Mallein-Gerin F. Functions of transforming growth factor-beta family type I receptors and Smad proteins in the hypertrophic maturation and osteoblastic differentiation of chondrocytes. J Biol Chem 2002;277:33545–58.
[48] Iwai T, Murai J, Yoshikawa H, Tsumaki N. Smad7 Inhibits chondrocyte differentiation at multiple steps during endochondral bone formation and down-regulates p38 MAPK pathways. J Biol Chem 2008;283:27154–64.

TISSUE ENGINEERING: Part A
Volume 18, Numbers 7 and 8, 2012

DOI: 10.1089/ten.tea.2011.0310

Magnesium Calcium Phosphate as a Novel Component Enhances Mechanical/Physical Properties of Gelatin Scaffold and Osteogenic Differentiation of Bone Marrow Mesenchymal Stem Cells

Ahmed Hussain, B.D.S., M.Sc.,[1] Kazuhisa Bessho, D.D.S., D.M.Sc.,[1] Katsu Takahashi, D.D.S., D.M.Sc.,[1] and Yasuhiko Tabata, Ph.D., D.Med.Sc., D.Pharm.[2]

Biodegradable gelatin sponges incorporating various amounts of magnesium calcium phosphate (MCP) were introduced and the *in vitro* osteogenic differentiation of rat bone marrow mesenchymal stem cells (MSCs) in the sponges was investigated. The MCP was added to the gelatin sponges at 0, 25, 50, 75, and 90 wt%. The pore sizes of the gelatin sponges ranged from 143 to 154.3 μm in diameter and the porosity percentage was 34.3–50.1%. The compression modulus of the sponges and the resistance to the volume change significantly increased with increases in the amount of MCP. When seeded into the sponges by an agitating method, MSCs were distributed throughout the sponges. Following the incubation of MSCs in the gelatin sponges, a significantly higher cellular proliferation and alkaline phosphatase activity was observed in the gelatin sponges incorporating higher MCP contents. On the other hand, the osteocalcin content of MSCs seeded in the gelatin sponges incorporating no or low MCP showed a significantly higher levels in comparison with the MSCs seeded in the gelatins incorporating high MCP. These findings indicate that the MCP incorporation maintained the pore size and porosity percentage of the gelatin sponges and enabled the sponge to achieve mechanical reinforcement as well as promoting MSC proliferation and osteogenic differentiation.

Introduction

LARGE BONE LOSS ASSOCIATED with trauma, tumor resection, and revision joint arthroplasty is a very challenging clinical problem. Currently, the gold standard for treating osseous defects is autogenous iliac crest bone grafting, with the major limitation of donor site morbidity in addition to the fact that the amount of bone available for autografting is limited.[1,2] To overcome these limitations, different types of bone scaffolds have been proposed. The scaffolds should posses essential characteristics including biocompatibility, osteoinductivity, osteoconductivity, interconnecting pore structure, appropriate mechanical properties, and degradability.[3,4]

Gelatin is one of the materials extensively used in biomedical fields. It is a biodegradable polymer that can be easily chemically modified and has been applied to pharmaceutical, medical, and food usage. We have prepared biodegradable hydrogels from different types of gelatin for the controlled release of various growth factors.[5] We also prepared gelatin sponges with or without tricalcium phosphate as a scaffold for bone regeneration to demonstrate that it is suitable for cell culture.[6]

Magnesium is the fourth most abundant cation in the human body and is naturally found in bone.[7] It is reported that magnesium is highly involved in bone formation and promotes cell attachment or spreading on other surfaces.[8] From the chemical view point, the presence of magnesium ions can reduce the crystallinity of calcium phosphate and increase the water solubility of phosphates.[9]

Different cells have been used to test the biological functions of scaffolds, among them, mesenchymal stem cells (MSCs) are clinically popular in regenerative medicine because they can be readily isolated from the bone marrow.[10] It is well recognized that MSCs have an inherent potential to differentiate into cell lineages of various types.[11] During the osteogenic differentiation of MSCs, it is known that cells differentiate into osteoprogenitors with a limited self-renewal capacity, then to preosteoblasts with limited proliferation, and finally mature into osteoblasts that secrete osteoid.[12]

The objective of this study was to evaluate the biological behavior of MSCs in gelatin sponges incorporating various amounts of magnesium calcium phosphate (MCP) and compare this with those without MCP. We also examine the physical and mechanical properties of the sponges.

[1]Department of Oral and Maxillofacial Surgery, Graduate School of Medicine, Kyoto University, Kyoto, Japan.
[2]Department of Biomaterials, Field of Tissue Engineering, Institute for Frontier Medical Sciences, Kyoto University, Kyoto, Japan.

Materials and Methods

Materials

Gelatin samples with an isoelectric point of 9.0 were kindly supplied by Nitta Gelatin Co. Calcium dihydrogen phosphate and magnesium oxide (90% and 99%, respectively) were obtained from Nacalai Tesque Ltd. and used without further purification. Culture media were obtained from Invitrogen Corporation (Carlsbad). Other chemicals were obtained from Wako Pure Chemical Industries.

Preparation of gelatin sponges incorporating MCP

Gelatin sponges containing different amounts of MCP were prepared by the dehydrothermal crosslinking of gelatin. Briefly, calcium dihydrogen phosphate and magnesium oxide at a molar ratio of 2:1[13] were mixed with 3 wt% of gelatin aqueous solution at different weight percentages of 0, 25, 50, 75, and 90 wt%. The mixed solution was agitated at 5,000 rpm for 3 min by using a homogenizer (ED-12; Nihonseiki Co.). The resulting foamy solution was cast into a polypropylene dish of $138 \times 138\,cm^2$ and 5 mm depth and then immediately frozen at −80°C. Finally, the sponges were freeze dried and dehydrothermally crosslinked at 140°C for 96 h.

Physical characterization of gelatin sponges incorporating MCP

The inner structure of sponges was viewed under a scanning electron microscope (SEM, S2380N; HITACHI), after sputter coating with gold/palladium. The porosity percentage and the mean diameter of the pores were determined by using ImageJ Version 1.43, Wayne Rasband, National Institute of Health.

The compression moduli of the freeze-dried gelatin sponges, with or without MCP incorporation ($5 \times 5 \times 5\,mm^3$), were measured by a mechanical apparatus (AG-5000B; Shimadzu) at a rate of 1 mm/min. A stress–strain curve was obtained and the compression moduli of samples were calculated from the initial slope of the load-deformation curve. Four sponges of each MCP concentration were used to calculate the average value and the standard deviation of the mean.

MSC preparation and culture

MSCs were isolated from the bone shaft of femurs of 3-week-old male Fisher 344 rats according to the technique reported by Lennon *et al.*[14] Briefly, both the ends of the femurs were cut away from the epiphysis and the bone marrow was flushed out by a syringe (21-gauge needle) with 1 mL of alpha-minimum essential medium supplemented with 15 vol.% fetal calf serum (FCS) and 50 IU/mL penicillin and streptomycin. The cell suspension (5 mL) was placed into T-75 culture flasks (SUMILON; Sumitomo Bakelite Co., Ltd.). The medium was changed every 3–4 days during culture. When the cells became subconfluent, they were detached by 0.25 wt% of trypsin, −0.02 wt% of ethylenediaminetetraacetic acid, and subcultured. Cells of the third passage at subconfluence were used for all the experiments.

MSC seeding into gelatin sponges incorporating MCP and culture

Gelatin sponges with or without MCP incorporation were cut into cylinders of 8-mm diameter and 1.25 ± 0.25 mm using a biopsy punch (Kai Industries Co. Ltd.). MSCs were homogenously seeded into the cylindrical sponges by the agitated seeding method as it has been demonstrated that this method is effective in seeding cells homogeneously throughout three-dimensional porous scaffolds.[15,16] Briefly, 50 μL of cell suspension (5×10^5 cells) was dropped on the sponges that had been placed into the wells of a 48-multiwell tissue culture plate (IWAKI Glass Co. Ltd.) and agitated on an orbital shaker (ORBITAL SHAKER; Bellco Glass, Inc.) at 180 rpm for 1 h. Then, 1 mL of culture medium was added and the shaking was continued for a further 5 h.

The cell-seeded sponges were placed into 6-well multiwell tissue culture plates (3815-012; IWAKI Glass Co. Ltd.). Each sponge was incubated in Dulbecco's modified Eagle medium supplemented with 15 vol.% FCS, 10 nM dexamethasone, 50 μg/mL ascorbic acid, and 10 mM β-glycerophosphate (osteogenic differentiation medium) at 37°C in a 5% CO_2–95% air atmosphere. The medium was changed and collected twice a week. The number of sponges used for each experimental group was 2 to 3.

SEM observation of MSCs cultured in gelatin sponges incorporating MCP

The gelatin sponges cultured with cells for 6 h were fixed with 2.5 wt% glutaraldehyde solution in 1× phosphate-buffered saline solution (PBS, pH 7.4). After PBS rinsing and subsequent dehydration with ethanol aqueous solutions, the dehydrated samples were immersed in t-butanol and dried with a critical point dryer (ES-2030; HITACHI). After sputter coating with gold/palladium, the samples were viewed on SEM.

Volume changes of the gelatin sponges incorporating MCP during culture

The change in the volume of gelatin sponges with or without MCP incorporation was determined by taking serial photographs of the scaffolds in the presence of a reference scale attached to the outside surface of the bottom of the culture dish, during the culture period. Image J software was used to calculate surface area of the scaffold and the reference scale. By correlating the size of the scaffold to the reference scale, it was possible to determine the dimensional change in the scaffold during the culture period. The photographs were taken with a digital camera (Cyber shot, DSC-F707; Sony).

Evaluation of cell behavior after incubation in gelatin sponges incorporating MCP

The number of MSCs attached to the gelatin sponges with or without MCP incorporation was determined by the fluorometric quantification of cellular DNA according to the method reported by Rao *et al.*[17] Briefly, the cell-seeded sponges were lysed in 500 μL of 30 mM sodium citrate–buffered saline solution (SSC) (pH 7.4) containing 0.2 mg/mL sodium dodecylsulfate by using a tissue lyser (Retsch Qiagen 85210 Tissue Lyser), for 10 min at 20 Hz, and then the samples were incubated at 37°C for 1 h. The cell lysate was centrifuged at 14,000 rpm and 4°C for 5 min to separate the cell lysate from the sponge remnants. The cell lysate (100 μL)

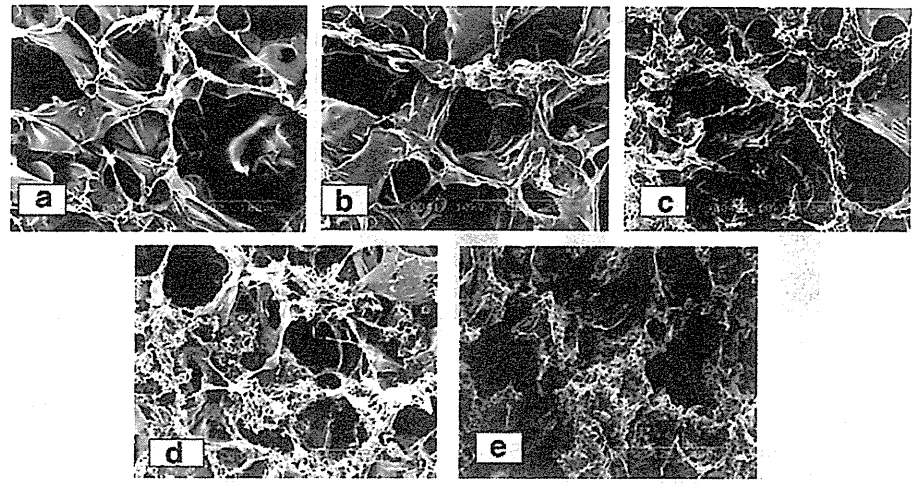

FIG. 1. Scanning electron micrographs of gelatin sponges incorporating 0 **(a)**, 25 **(b)**, 50 **(c)**, 75 **(d)**, and 90 wt% of MCP **(e)**. MCP, magnesium calcium phosphate.

was mixed with a dye solution (100 μL; 30 mM SSC, 1 μg/mL Hoechst 33258 dye) and the fluorescent intensity of the mixed solution was measured in a fluorescence spectrometer (F-2000; HITACHI) at excitation and emission wavelengths of 355 and 460 nm, respectively. The calibration curve between the DNA and cell number was prepared by using cells of known numbers.

As a measure of MSC osteogenic differentiation, the alkaline phosphatase (ALP) activity and osteocalcin content were determined. The ALP of cells was determined by using the conventional p-nitrophenylphosphate method,[18] while the osteocalcin content of the cells was determined by the enzyme-linked immunosorbent assay (ELISA) method. Briefly, MSCs cultured in the sponges for different time periods were mixed with 1 mL of 40 vol.% formic acid for more than 12 h to decalcify them using a mixer (CM-1000; Eyela Co. Ltd.). After the decalcified samples were centrifuged, the supernatant of the cell extraction was applied to gel filtration on a SephadexTM G-25 column (PD-10; Amersham Pharmacia Biotech AB). The resulting solution was freeze dried, redissolved in double distilled water (DDW), and subjected to an osteocalcin rat ELISA (Rat osteocalcin ELISA system; Biomedical Technologies Inc.).

Evaluation of the magnesium concentration in culture medium

The collected cultured media were freeze dried. The freeze-dried powder was then redissolved with DDW in a similar volume to that of the culture medium originally collected to ensure that all the samples had the same volume. The magnesium was determined by using the xylidyle blue method (Magnesium B reagent Kit; Wako Pure Chemical Industries) and standardized by the culture medium of the 0 wt% scaffolds. Briefly, 5 μL of culture medium was mixed with 750 μL of color reagent. Absorbance was measured at 520 nm.

Statistical analysis

All the data were analyzed by one-way analysis of variance with Tukey's test to compare significance, and statistical significance was accepted at $p<0.05$. Graph Pad Prism 5 software was used to conduct the statistical analysis. Experimental results were expressed as the mean+standard deviation.

Results

Characterization of gelatin sponges incorporating MCP

Figure 1 shows scanning electron micrographs of gelatin sponges with or without MCP incorporation. Irrespective of the MCP content, a similar infrastructure was observed, where the MCP appeared to be incorporated uniformly into the matrix of the gelatin sponges and deposited within the wall of every sponge. All the sponges had an interconnected porous structure with the pore size ranging from 143 to 154 μm, while the porosity percentages were around 34.3–50.1% (Table 1). The compression modulus of the sponges increased significantly with increases in the amount of MCP incorporated. For example, the compression modulus of the gelatin sponges containing 75 and 90 wt% MCP was significantly different from those incorporating lower amounts of MCP (Fig. 2).

The gelatin sponges containing MCP showed an initial burst of magnesium followed by a steady-release profile. On the other hand, the gelatin sponges incorporating 90 wt% MCP showed a significantly higher release profile over the whole culture period in comparison with the other sponges (Fig. 3).

TABLE 1. CHARACTERIZATION OF GELATIN SPONGES WITH OR WITHOUT MAGNESIUM CALCIUM PHOSPHATE INCORPORATION

MCP wt%	*Mean pore diameter (μm)*	*Porosity (%)*
0	153.0±60.72	44.±2.6
25	154.3±30.8	44.2±3.8
50	139.9±37.1	33.3±2.0
75	152.2±30.5	50.1±4.2
90	143.0±48.2	34.3±1.8

There is no significant difference among groups.
MCP, magnesium calcium phosphate.

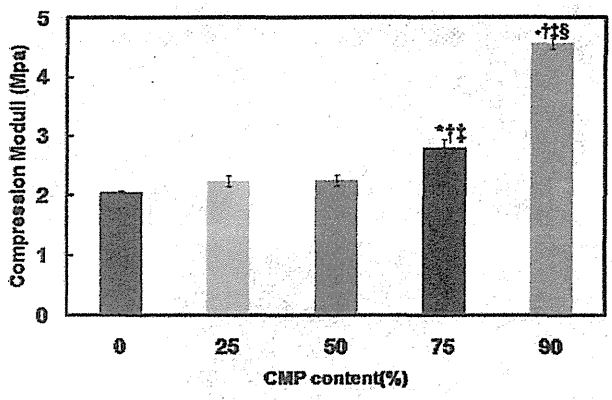

FIG. 2. Compression moduli of gelatin sponges incorporating different MCP contents. $^{*}p<0.05$; significant against the compression modulus of gelatin sponges incorporating 0 wt% of MCP. $^{\dagger}p<0.05$; significant against the compression modulus of gelatin sponges incorporating 25 wt% of MCP. $^{\ddagger}p<0.05$; significant against the compression modulus of gelatin sponges incorporating 50 wt% of MCP. $^{\S}p<0.05$; significant against the compression modulus of gelatin sponges incorporating 75 wt% of MCP.

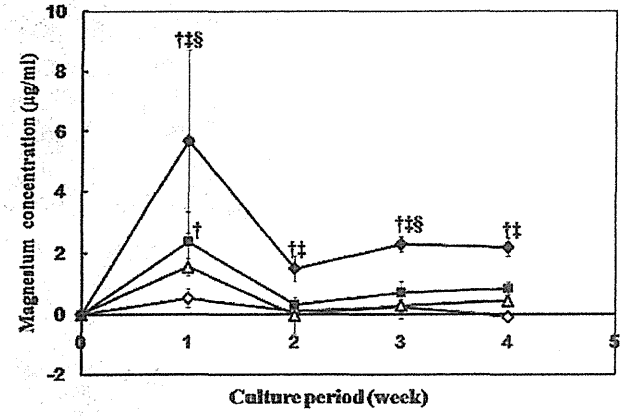

FIG. 3. Magnesium concentration in the medium after culturing with gelatin sponges incorporating 25 (◇), 50 (Δ), 75 (■), and 90 (◆) of MCP content. $^{\dagger}p<0.05$; significant against magnesium concentration of the medium of gelatin sponges incorporating 25 wt% of MCP. $^{\ddagger}p<0.05$; significant against magnesium concentration of the medium of gelatin sponges incorporating 50 wt% of MCP. $^{\S}p<0.05$; significant against magnesium concentration of the medium of gelatin sponges incorporating 75 wt% of MCP.

Attachment and proliferation of MSCs in gelatin sponges incorporating MCP

Figure 4 shows SEM photographs of gelatin sponges incorporating MCP 6 h after MSC seeding. The cells attached to all types of sponges and they were distributed throughout the sponges. No difference in the shape of the attached MSCs was observed among sponges.

Volume change of gelatin sponges incorporating MCP

Figure 5 shows the percent change in the volume of the gelatin sponges incorporating MCP. The dimensional stability of gelatin sponges incorporating MCP seemed to increase in proportion to the amount of MCP. The gelatin sponges incorporating 90 wt% MCP showed the highest dimensional stability; about 88.7% of the initial size was maintained even after 4 weeks of culture. On the other hand, the gelatin sponges containing 0 wt% of MCP showed the least dimensional stability.

MSC proliferation and osteogenic differentiation in gelatin sponges incorporating MCP

Figure 6 shows the number of MSCs proliferated in the gelatin sponges with or without MCP incorporation. In the first week of culture, no significant difference was seen in the cell number among different types of sponges. On the contrary, 2 weeks later, the gelatin sponges incorporating 90 wt% MCP showed a significant increase in the cell number compared with the other sponges. In the third and fourth week of culture, the cell number significantly increased for the sponges incorporating 75 and 90 wt% MCP in comparison with others. The cells seeded in the gelatin sponges incorporating 50 wt% MCP showed a significant difference only in the fourth week of

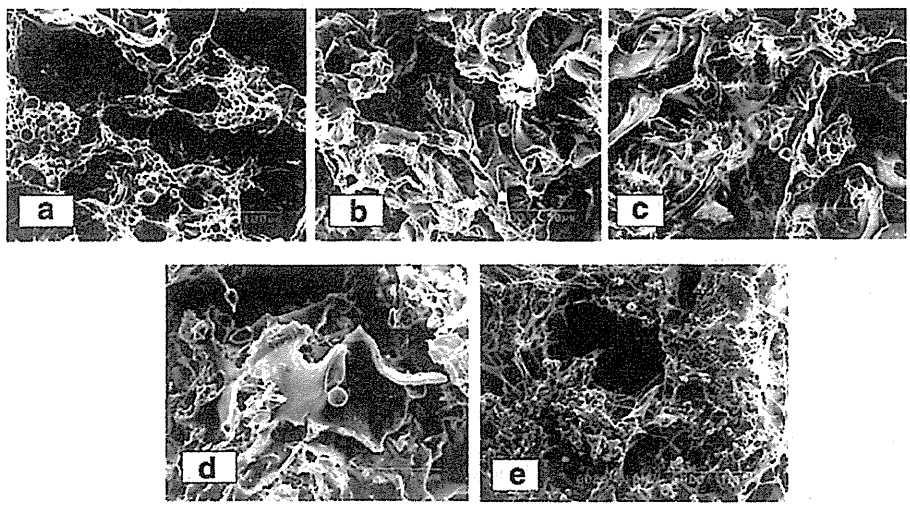

FIG. 4. Scanning electron micrographs of MSCs attaching to gelatin sponges incorporating 0 **(a)**, 25 **(b)**, 50 **(c)**, 75 **(d)**, and 90 wt% of MCP **(e)**. MSCs, mesenchymal stem cells.

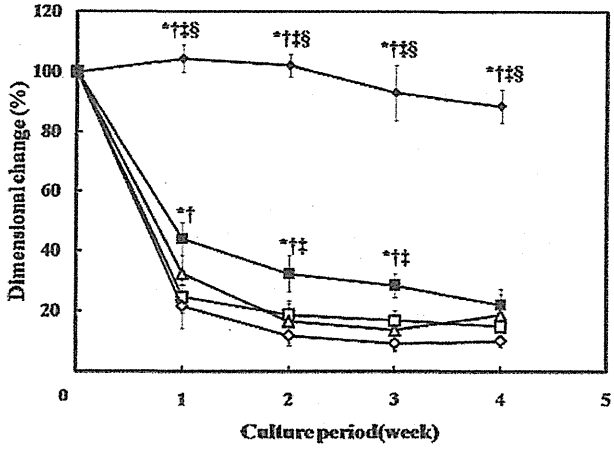

FIG. 5. Percent change in the volume of the gelatin sponges incorporating 0 (□), 25 (◇), 50 (Δ), 75 (■), and 90 wt% (◆) of MCP contents. *$p < 0.05$; significant against the volume change of gelatin sponges incorporating 0 wt% of MCP. †$p < 0.05$; significant against the volume change of gelatin sponges incorporating 25 wt% of MCP. ‡$p < 0.05$; significant against the volume change of gelatin sponges incorporating 50 wt% of MCP. §$p < 0.05$; significant against the volume change of gelatin sponges incorporating 75 wt% of MCP.

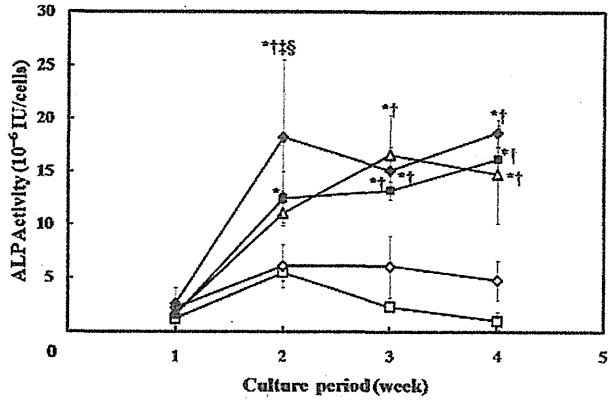

FIG. 7. Time course of the ALP activity of MSCs in the gelatin sponge incorporating 0 (□), 25 (◇), 50 (Δ), 75 (■), and 90 (◆) of MCP content. *$p < 0.05$; significant against the ALP activity of the cells in gelatin sponges incorporating 0 wt% of MCP. †$p < 0.05$; significant against the ALP activity of the cells in gelatin sponges incorporating 25 wt% of MCP. ‡$p < 0.05$; significant against the ALP activity of the cells in gelatin sponges incorporating 50 wt% of MCP. §$p < 0.05$; significant against the ALP activity of the cells in gelatin sponges incorporating 75 wt% of MCP. ALP, alkaline phosphatase.

culture compared with those seeded in gelatin sponges incorporating lower amounts of MCP.

Figure 7 shows the time course of the ALP activity of MSCs after culture in gelatin sponges with or without MCP. In the second week of culture, the ALP activity of the MSCs cultured in the gelatin sponges incorporating 90 wt% MCP was significantly higher than that of the other gelatin sponges. In the third and fourth week of culture, the MSCs cultured in the gelatin sponges incorporating 50, 75, and 90 wt% MCP showed a significantly higher ALP activity in comparison with the other groups.

The osteocalcin content of MSCs cultured in the gelatin sponges containing 0 or 25 wt% of MCP was significantly higher when compared with those of the gelatin sponges containing 75 and 90 wt% of MCP, in the fourth week of culture (Fig. 8).

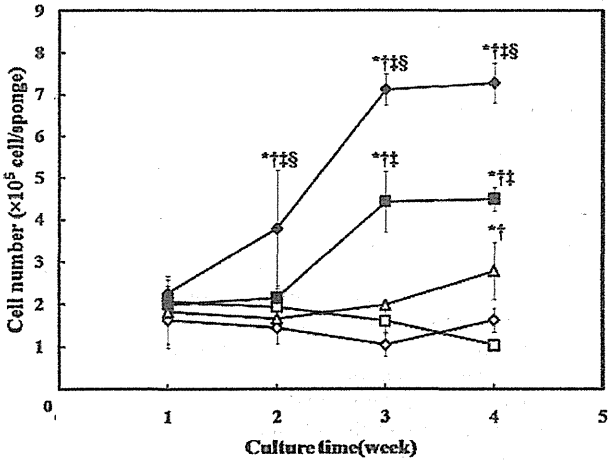

FIG. 6. Time course of MSC proliferation in gelatin sponges incorporating 0 (□), 25 (◇), 50 (Δ), 75 (■), and 90 (◆) of MCP content. *$p < 0.05$; significant against MSC number in the gelatin sponge incorporating 0 wt% of MCP. †$p < 0.05$; significant against MSC number in the gelatin sponge incorporating 25 wt% of MCP. ‡$p < 0.05$; significant against MSC number in the gelatin sponge incorporating 50 wt% of MCP. §$p < 0.05$; significant against MSC number in the gelatin sponge incorporating 75 wt% of MCP.

Discussion

This study investigated the proliferation and osteogenic differentiation of MSCs in gelatin sponges incorporating

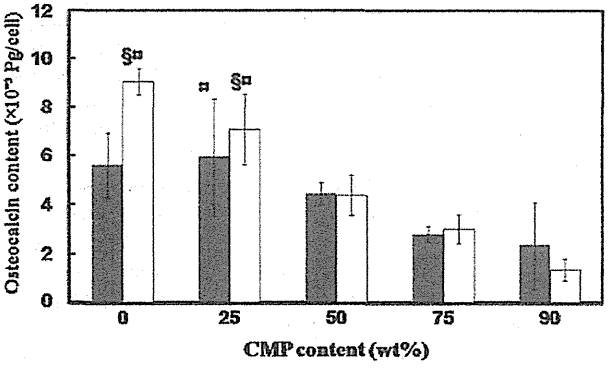

FIG. 8. Osteocalcin content of the MSCs in the gelatin sponge containing different MCP contents at 2 weeks (black column) and 4 weeks (white column). §$p < 0.05$; significant against the osteocalcin content of the cells in the gelatin sponges incorporating 75 wt% of MCP. ¤$p < 0.05$; significant against the osteocalcin content of the cells in the gelatin sponges incorporating 90 wt% MCP.

different amounts of MCP or without MCP incorporation. Incorporation of MCP enabled the gelatin sponges to mechanically reinforce and promote the proliferation and osteogenic differentiation of MSCs. The gelatin sponges incorporating MCP could be prepared by an easy, one-step procedure with the advantage of creating a porous structure for cell-based bone regeneration. In other words, the simple foaming of a gelatin solution permitted the formation of gelatin sponges, while the addition of MCP improved the physical, mechanical, and biological properties of the sponges. The sponges also showed slow magnesium release, which may contribute to bone regeneration *in vivo*.[7] In addition, the gelatin used in the sponge fabrication, I.P.9 gelatin, is a known carrier for bone morphogenetic protein-2,[19] an important osteoinductive and ectopic bone-forming protein.[20]

There is growing consensus that the physical properties of materials, such as topography, geometry, porosity, and stiffness, can be used to direct biological outcomes in a manner similar to traditional approaches involving chemistry or biomolecules.[21]

The addition of MCP to the gelatin sponges did not affect their porosity percentage and pore size because the MCP was added during, not after, the sponge fabrication. In other words, the MCP was mixed during the gelatin foaming procedure with the end result of no difference in pore size and porosity percentage among groups. On the contrary, the compression modulus increased with the addition of MCP (Fig. 2), which is of great value for the regeneration of hard tissue such as bone.[4] The cells cultured in the gelatin sponges with or without MCP incorporation did not show a different morphology (Fig. 4), indicating that MCP has no negative effect on cell morphology.

When MSCs were cultured in the gelatin sponges incorporating MCP, the number of MSCs proliferating in the sponges increased with increases in the amount of MCP. For example, there was an eightfold increase in the MSC number cultured in the gelatin sponges incorporating 90 wt% MCP compared with those of MCP-free sponges (Fig. 6). This can be explained in terms of pore space in the sponges. As shown in Figure 5, although the initial sponge size and porosity were almost the same for all the groups, they were deformed during the culture period, and since the gelatin sponges with higher amounts of MCP incorporated showed less shrinkage, there was more room for the cells in these sponges to grow and multiply, with more surface area exposed to oxygen and nutrients.[6] Another possible reason is the dissolution of magnesium and calcium ions, which can stimulate cellular proliferation.[22,23]

The ALP activity of MSCs in the sponges increased with increases in the amount of MCP; for example, the ALP activity in the gelatin sponges incorporating 90 wt% MCP showed a threefold increase in the second week of culture. This could be due to the presence of calcium and phosphate with magnesium, which is known to facilitate cell differentiation.[24–29] In addition, the differentiation of cells was maximized when the modulus of the scaffold increased to match that of bone tissue.[30] Another possible reason is the change in surface topography, as seen in Figure 4, where 90 wt% gelatin sponges shown a rough microscopic morphology in comparison with 0 wt%. Rough surfaces have been showed to enhance osteogenic differentiation in comparison with smooth surfaces.[31]

Osteocalcin, a late osteo-differentiation marker, showed a higher amount per cell in the gelatin scaffold incorporating low or no MCP. This could be explained by the fact that the cells in the gelatin sponges containing a high MCP content are at the early stage of osteogenic differentiation, which is characterized by a high proliferation index and ALP activity. Meanwhile, the cells in the low or without MCP gelatin sponges are at the late osteogenic differentiation stage, which is characterized by low cell proliferation, low ALP, and high osteocalcin levels.[32,33] The dimensional shrinkage, which limits cellular proliferation and enhances contact differentiation of MSCs, could be a possible explanation for the high osteocalcin levels in the gelatin sponges with low MCP content. On the other hand, a high magnesium concentration has been known to have an inhibitory action on late osteogenic differentiation by increasing the expression of the anticalcification protein osteopontin with upregulation of the calcification inhibitor, matrix Gla protein.[34]

In summary, the addition of MCP did not affect the pore size and porosity percentage adversely. Moreover, it improved the dimensional stability and compression modulus of the gelatin scaffolds, which in turn along with the slow magnesium release and surface roughness promoted MSC proliferation and osteogenic differentiation.

Conclusion

Novel scaffolds based on gelatin and MCP were introduced. The addition of MCP to the gelatin sponges during preparation did not reduce the pore size and porosity percentage of the scaffold. Furthermore, a significant increase in dimensional stability and compression modulus was identified in the sponges containing high amount of MCP.

The MSCs seeded into the gelatin sponges containing MCP showed consistency in morphology with those without MCP content. In addition, the MSC proliferation and osteogenic differentiation benefited greatly by the increase in dimensional stability, hardness, roughness, and magnesium release in the gelatin sponges containing MCP.

Disclosure Statement

No competing financial interests exist.

References

1. Colterjohn, N.R., and Bednar, D.A. Procurement of bone graft from the iliac crest. An operative approach with decreased morbidity. J Bone Joint Surg Am **79,** 756, 1997.
2. Kneser, U., Schaefer, D.J., Polykandriotis, E., and Horch, R.E. Tissue engineering of bone: the reconstructive surgeon's point of view. J Cell Mol Med **10,** 7, 2006.
3. Salgado, A.J., Coutinho, O.P., and Reis, R.L. Bone tissue engineering: state of the art and future trends. Maccromol Biosci **4,** 743, 2004.
4. Hutmacher, D.W. Scaffold design and fabrication technologies for engineering tissue—state of the art and future perspectives. J Biomater SciPolym Ed **12,** 107, 2001.
5. Tabata, Y. Tissue regeneration based on growth factor release. Tissue Eng **9 (Suppl 1),** S5, 2003.
6. Takahashi, Y., Yamamoto, M., and Tabata, Y. Osteogenic differentiation of mesenchymal stem cells in biodegradable sponges composed of gelatin and β-tricalcium phosphate. Biomaterials **26,** 3587, 2005.

7. Straiger, M.P., Pietak, A.M., Huadmai, J., and Kas, G. Magnesium and its alloys as orthopedic biomaterials: review. Biomaterials **27,** 1728, 2006.
8. Revel, P.A., Damien, E., Zhang, X.S., Evans, P., and Howlett, C.R. The effect of magnesium ion on bone bonding to hydroxyapatite coating on titanium alloy implants. Bioceramics **254,** 447, 2004.
9. Marchi, J., Dantas, A.C., Greil, P., Bressiani, J.C., Bressiani, A.H., and Muller, F.A. Influence of Mg-substitution on the physicochemical properties of calcium phosphate powders. Mater Res Bull **42,** 1040, 2007.
10. Lennon, D.P., Haynesworth, S.E., Arm, D.M., Baber, M.A., and Caplan, A.I. Dilution of human mesenchymal stem cells with dermal fibroblasts and the effects on *in vitro* and *in vivo* osteochondrogenesis. Dev Dyn **219,** 50, 2000.
11. Grigoriadis, A.E., Heersche, J.N., and Aubin, J.E. Differentiation of muscle, fat, cartilage, and bone from progenitor cells present in a bone-derived clonal cell population: effect of dexamethasone. J Cell Biol **106,** 2139, 1988.
12. Aubin, J.E., and Triffitt, J.T. Mesenchymal stem cells and osteoblast differentiation. In: John, P.B., Lawrence, G.R., Gideon, A.R., eds. Principles of Bone Biology, 2nd edition. San Diego: Academic Press, 2002, pp. 59–81.
13. Junfeng, J., Huanjun, Z., Jie, W., Xin, J., Hong, H., and Fangping *et al.* Development of magnesium calcium phosphate biocement for bone regeneration. J Roy Soc Interface **7,** 1171, 2010.
14. Lennon, D.P., Haynesworth, S.E., Young, R.G., Dennis, J.E., and Caplan, A.L. A chemically defined medium supports *in vitro* proliferation and maintains the osteochondral potential of rat marrow-derived mesenchymal stem cells. Exp Cell Res **219,** 211, 1995.
15. Kim, B.S., Nikolovski, J., Bonadio, J., Smiley, E., and Mooney, D.J. Engineered smooth muscle tissues: regulating cell phenotype with the scaffold. Exp Cell Res **251,** 318, 1999.
16. Takahashi, Y., and Tabata, Y. Homogeneous seeding of mesenchymal stem cells into nonwoven fabric for tissue engineering. Tissue Eng **9,** 931, 2003.
17. Rao, J., and Otto, W.R. Fluorimetric DNA assay for cell growth estimation. Anal Biochem **207,** 186, 1992.
18. Kobayashi, D., Takita, H., Mizuno, M., Totsuka, Y., and Kuboki, Y. Time-dependent expression of bone sialoprotein fragments in osteogenesis induced by bone morphogenetic protein. J Biochem **119,** 475, 1996.
19. Yamamoto, M., Takahashi, Y., and Tabata, Y. Controlled release by biodegradable hydrogels enhances the ectopic bone formation by bone morphogenetic protein. Biomaterials **24,** 4375, 2003.
20. Bessho, K., Konishi, Y., Kaihara, S., Fujimura, K., Okubo, Y., and Iizuka, T. Bone induction by *Escherichia coli*-derived recombinant human bone morphogenetic protein-2 compared with Chinese hamster overy cell-derived recombinant human bone morphogenetic protein-2. Brit J Oral Maxillofac Sug **38,** 645, 2000.
21. Engler, A., Sen, S., Sweeney, H., and Discher, D. Matrix elasticity directs stem cell lineage specification. Cell **126,** 677, 2006
22. Dietrich, E., Oudadesse, H., Lucas-Girot, A., and Mami, M. *In vitro* bioactivity of melt- derived glass 46S6 doped with magnesium. J Biomed Mater Res A **88,** 1087, 2009.
23. Sader, M.S., LeGeros, R.Z., and Soares, G.A. Human osteoblasts adhesion and proliferation on magnesium substituted tricalcium phosphate dense tablets. J Mater Sci Mater Med **20,** 521, 2009.
24. Jingxiong, L., Jie, W., Yonggang, Y.,Hong, L., Junfeng, J., and Shicheng, *et al.* Preparation and preliminary cytocompatibility of magnesium doped apatite cement with degradability for bone regeneration. J Mater Sci Mater Med **22,** 607, 2011.
25. Sodek, J., and Cheifetz, S. Molecular regulation of osteogenesis. In: Davies, J.E., ed. Bone Engineering. Toronto: EM Squared Inc., 2000.
26. Dietrich, E., Oudadesse, H., Lucas-Girot, A., and Mami, M. *In vitro* bioactivity of melt-derived glass 46S6 doped with magnesium. J Biomed Mater Res A **88,** 1087, 2009.
27. Sun, H.L., Wu, C.T., Dai, K.R., Chang, J., and Tang, T.T. Proliferation and osteoblastic differentiation of human bone marrow-derived stromal cells on akermanite-bioactive ceramics. Biomaterials **27,** 5651, 2006.
28. Qi, G.C., Zhang, S., Khor, K.A., Lye, S.W., Zeng, X.T., and Weng, *et al.* Osteoblastic cell response on magnesium-incorporated apatite coatings. Appl Surf Sci **255,** 304, 2008.
29. Feyerabend, F., Witte, F., Kammal, M., and Willumeit, R. Unphysiologically high magnesium concentrations support chondrocyte proliferation and redifferentiation. Tissue Eng **12,** 3545, 2006.
30. Chatterjee, K., Lin-Gibson, S., Wallace W., Parekh, S., Lee, Y., Cicerone, M. Young M., and Simon, C. The effect of 3D hydrogel scaffold modulus on osteoblast differentiation and mineralization revealed by combinatorial screening. Biomaterials **31,** 5051, 2010.
31. Vandrovcová, M., and Bačáková, L. Adhesion, growth and differentiation of osteoblasts on surface- modified materials developed for bone implants. Physiol Res **60,** 403, 2011.
32. Aubin, J.E. Regulation of osteoblast formation and function. Rev Endocr Metab Disord **2,** 81, 2001.
33. Witte, F., Feyerabend, F., Maier, P., Fischer, J., Stormer, M., and Balwert *et al.* Biodegradable magnesium-hydroxyapatite metal matrix composites. Biomaterials **28,** 2163, 2007.
34. Montezano, A., Zimmerman, D., Yusuf, H., Burger, D., Chignalia, A., Wadhera, V., van Leeuwen, F., and Touyz, R. Vascular smooth muscle cell differentiation to an osteogenic phenotype involves TRPM7 modulation by magnesium. Hypertension **56,** 453, 2010.

Address correspondence to:
Ahmed Hussain, B.D.S., M.Sc.
Department of Oral and Maxillofacial Surgery
Graduate School of Medicine
Kyoto University
54 Kawahara-cho
Shogoin
Sakyo-ku
Kyoto 606-8507
Japan

E-mail: frontierscientist@gmail.com

Received: May 30, 2011
Accepted: October 13, 2011
Online Publication Date: December 9, 2011

J Oral Maxillofac Surg
70:1170-1173, 2012

Rigid Fixation of Intraoral Vertico-Sagittal Ramus Osteotomy for Mandibular Prognathism

Kazuma Fujimura, DDS, PhD, and*
Kazuhisa Bessho, DDS, PhD†

The standard surgical treatment for prognathism is sagittal split ramus osteotomy (SSRO) if the proximal and distal segments of the ramus require fixing with screws or metal plates. In this procedure, however, it is frequently difficult to avoid neurosensory disturbance (NSD) of the inferior alveolar nerve (IAN) when the posterior margin of the ramus curves inward or when the ramus is thin (Fig 1A, B). This report describes a new alternative procedure, intraoral vertico-sagittal ramus osteotomy (IVSRO),[1] a modification of SSRO and intraoral vertical ramus osteotomy (IVRO). One of the main advantages of IVSRO is that it avoids IAN damage, because the ramus can be split parallel to the original sagittal plane posterior to the point between the mandibular canal and the lateral cortical bone plate immediately in front of the antilingular prominence. Another advantage of IVSRO is that the area in which screws can be inserted is relatively large, if the subcoronoid area on the distal segment and subcondylar area on the proximal segment are used. The 2 segments can be fixed in these areas with bicortical bone screws, with or without a cheek incision (Fig 1C). This report introduces rigid fixation of IVSRO for mandibular prognathism.

Received from the Department of Oral and Maxillofacial Surgery, Graduate School of Medicine, Faculty of Medicine, Kyoto University, Kyoto, Japan.

*Associate Professor.

†Professor and Chair.

Address correspondence and reprint requests to Dr Fujimura: Department of Oral and Maxillofacial Surgery, Graduate School of Medicine, Faculty of Medicine, Kyoto University, 54 Kawahara, Sakyo-ku, Kyoto 606-8507, Japan; e-mail: fujimura@kuhp.kyoto-u.ac.jp

Published by Elsevier Inc on behalf of the American Association of Oral and Maxillofacial Surgeons
0278-2391/12/7005-0$36.00/0
doi:10.1016/j.joms.2011.03.010

Technique

Osteotomy of the ramus in IVSRO is a modified version of straight IVSRO and extended IVSRO for advancement of the mandible.[1] Briefly, the lateral aspect is exposed from the sigmoid notch to the antegonial notch. To avoid damaging the IAN and the maxillary artery, the medial aspect of the ramus may also be exposed carefully from the sigmoid notch area to the lingula and the posterior border of the ramus,[2] as in SSRO. To avoid a fracture or bad split, the full thickness of the sigmoid notch is cut with a fissure burr, reciprocating saw, or oscillating saw inferiorly along the planed decortication line until the bone marrow is exposed. This process, full-thickness cutting of the sigmoid notch, is the most important and most technically difficult step of the IVSRO procedure. A wedge-shaped decortication of the lateral aspect of the ramus from the sigmoid notch to the antegonial notch is performed using a flat-top, cylindrical fissure burr parallel to the original sagittal plane until the bone marrow is exposed.[3] A bone spatula and an osteotom are used for vertical osteotomy along almost the entire sagittal plane to the medial posterior border of the ramus. The distal segment is then repositioned posteriorly, and intermaxillary fixation (IMF) is performed. The inner aspect of the decorticated distal segment is spontaneously overlapped with the proximal segment. The subcoronoid area and the subcondylar area in each segment are also overlapped. The 2 segments can be fixed using bicortical bone screws. If possible, a 90° screwdriver system (eg, angled drilling system and insertion screws, 12-mm screw length; http://www.Synthes.com) is used with an intraoral procedure (Fig 2A-C). When the 2 segments are fixed rigidly, IMF is usually not required after surgery. However, a favorable outcome is usually obtained with IMF for about 3 days to prevent postoperative bleeding and to aid in wound healing. To stabilize the occlusion postoperatively, intermaxillary elastics are applied for about 2 months after release of IMF.

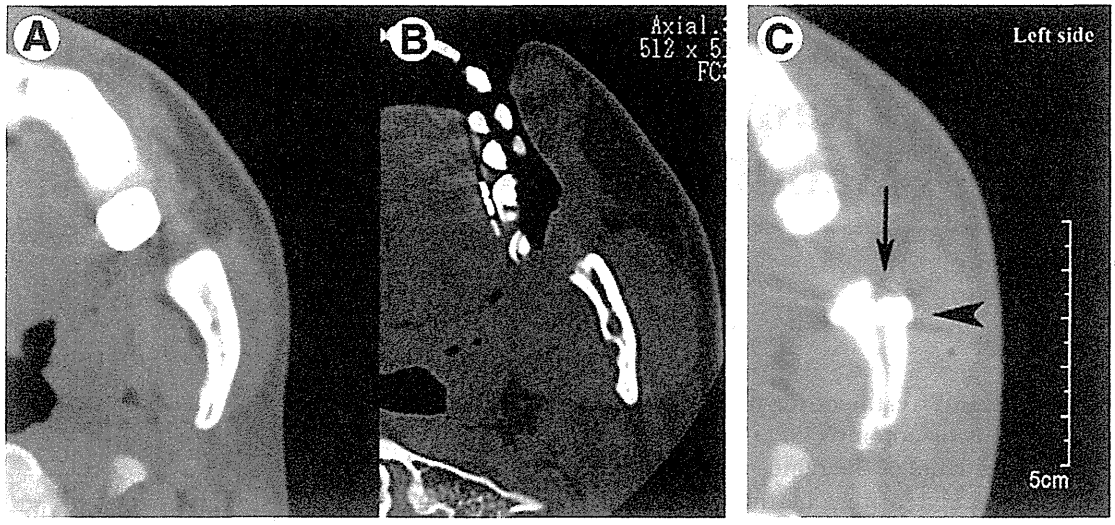

FIGURE 1. Axial computed tomographic film of the left mandibular ramus. *A, B,* Preoperative images. Sagittal split ramus osteotomy is more difficult if the posterior border of the mandibular ramus curves inward or the ramus is thin. *C,* Postoperative image of rigid fixation with screws in *A*. The anterolateral cortical bone of the proximal segment is removed (*arrow*) and osteotomy is performed from a point between the mandibular canal and the lateral cortical bone. The proximal and distal segments are fixed using bicortical bone screws (*arrowhead*).

Fujimura and Bessho. Rigid Fixation of IVSRO. J Oral Maxillofac Surg 2012.

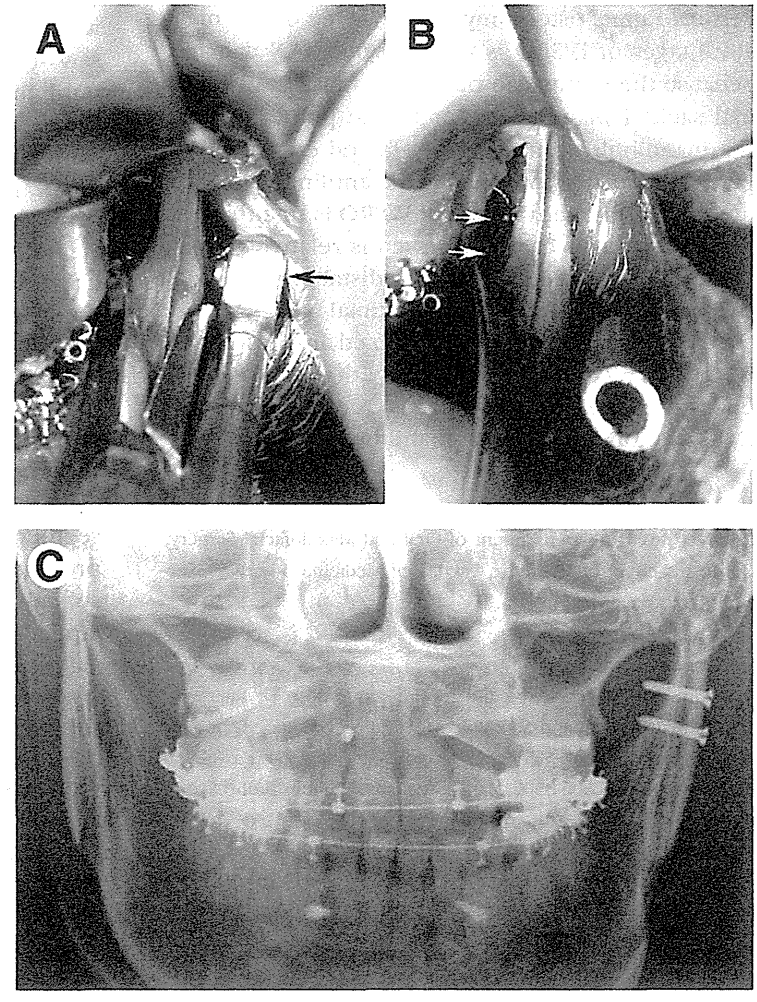

FIGURE 2. Intraoral vertico-sagittal ramus osteotomy. *A,* A 90° screwdriver system (*arrow*) (angled drilling system; http://www.Synthes.com) and *B,* insertion screws (*arrows*) (2.4 mm in diameter, 12-mm screw length) were used for the intraoral procedure. *C,* Postoperative image. The distal segment of the mandible was rotated to the left side for mandibular deformity, and rigid fixation was performed in only the setback side.

Fujimura and Bessho. Rigid Fixation of IVSRO. J Oral Maxillofac Surg 2012.